Characterisation of wood properties and transverse anatomy for vacuum drying modelling of commercially important Australian hardwood species

Denis M Cullity Research Fellowship Report

Adam Lloyd Redman
Research Scientist, Innovative Forest Products
Department of Primary Industries and Fisheries

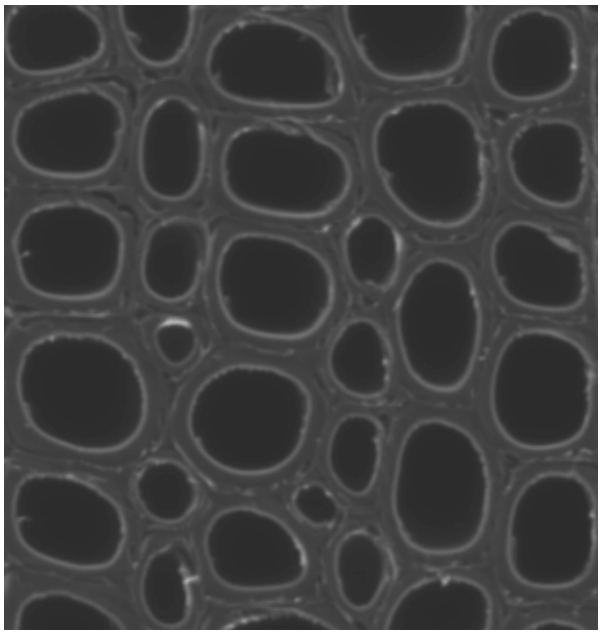

Forest and Wood Products Australia
Report Number PG08.5097

Forest&Wood Products Australia

Queensland Government
Department of Primary Industries and Fisheries

AgroParisTech ENGREF
INSTITUT DES SCIENCES ET INDUSTRIES DU VIVANT ET DE L'ENVIRONNEMENT
PARIS INSTITUTE OF TECHNOLOGY FOR LIFE, FOOD AND ENVIRONMENTAL SCIENCES

Preface

The Denis M Cullity Fellowship was established by the Forest and Wood Products Research & Development Corporation, the predecessor entity of Forest and Wood Products Australia Ltd, in 2000 in honour of the Corporation's inaugural Chairman Mr Denis M Cullity CMG AO.

The Fellowship is intended to support professional development of leading Australian forestry or forest product scientists and increase the value and benefits derived from research completed for the forestry products industry.

For further information on the Fellowships contact Forest and Wood Products Australia:

Suite 607, Level 6 Yarra Tower, World Trade Centre
Melbourne, VIC 3005

PO Box 69, World Trade Centre
VIC 8005

Tel : (03) 9614 7544
Fax : (03) 9614 6822
Email : info@fwpa.com.au
Webpage : www.fwpa.com.au

Financial and In-kind Contributors

The substantial contributions of AgroParisTech University - l'École Nationale du Génie Rural des Eaux des Forêts (ENGREF), Queensland University of Technology (QUT), Forest and Wood Products Australia (FWPA) and the Department of Primary Industries and Fisheries (DPI&F), to the successful undertaking of this collaborative project are gratefully acknowledged.

Acknowledgements

Dr Patrick Perré, Professor, Head of LERMAB (Integrated research unit on wood science), AgroParisTech – ENGREF France

Dr Françoise Huber, Research Engineer, INRA France

Dr Romain Remond, Research Engineer, AgroParisTech – ENGREF France

Dr Giana Almeida, Post Doctorate, ESALQ Brazil.

Patrice Marchal, Research Technician, AgroParisTech – ENGREF France

Floran Pierre, PHD Student, AgroParisTech – ENGREF France

Mariella De La Cruz-Lefevre, PHD Student, AgroParisTech – ENGREF and FCBA, France

Jean Claude Mosnier, Forest Technician, AgroParisTech – ENGREF France

Dr Ian Turner, Professor, School of Mathematical Sciences QUT, Australia

Ingo Wollocha, Sales Manager Brunner-Hildebrand, Germany

Dr Henri Bailleres, Research Scientist Innovative Forest Products, DPI&F Australia.

Robert McGavin, Research Scientist Innovative Forest Products, DPI&F Australia.

Martin Davies, Research Technician Innovative Forest Products, DPI&F Australia.

Board members of FWPA (2008), Australia.

Summary

Objective

This Denis M Cullity Fellowship report is supported by FWPA, DPI&F, ENGREF and QUT. The result of the fellowship underpins the predictive modelling section of the FWPA project PN08.2047 - Evaluation of super-heated steam vacuum drying viability and development of a predictive drying model for Australian commercial hardwood species.

The principle objective for this fellowship was, through exposure to overseas skills and processes, to gain a better understanding of the wood properties that explain the drying behaviour of the main commercial Australian hardwoods for future development of a vacuum drying model for these species. This was achieved by utilising 'state of the art' equipment to acquire intrinsic wood property and transverse anatomy data at AgroParisTech – ENGREF, France. In brief, the following research was undertaken:

- ESEM (environmental scanning electron microscope) scans and subsequent image analysis of each species to characterise cell morphology,
- DMA (dynamic mechanical analysis) analysis to investigate viscoelastic behaviour of each species in the tangential and radial directions,
- wood water relationship measurements on micro samples involving a highly sensitive microbalance and laser technology to accurately measure loss of moisture content in conjunction with directional shrinkage.

The species investigated were: *Corymbia citriodora* (spotted gum), *Eucalyptus pilularis* (blackbutt), *Eucalyptus marginata* (jarrah) and *Eucalyptus obliqua* (messmate).

Key Results

Characterisation and investigation of a number of key wood properties, critical for further modelling work, has been achieved. The key results were:

- Morphological characterisation, in terms of fibre cell wall thickness and porosity, was completed. A clear difference in fibre porosity, size, wall thickness and orientation was evident between species. Results were consistent with published data for other species.
- Viscoelastic properties of wood were shown to differ greatly between species and in the radial and tangential directions, largely due to anatomical and chemical variations. Consistent with published data, the radial direction shows higher stiffness, internal friction and glass transition temperature than the tangential directions. The loss of stiffness over the measured temperature range was greater in the tangential direction than the radial direction. Due to time dependant molecular relaxation, the storage modulus and glass transition temperature decreased with decreasing test frequency,

approaching an asymptotic limit. Thus the viscoelastic properties measured at lower frequencies are more representative of static material.

- Dynamic interactions between relative humidity, moisture content and shrinkage of four Australian hardwood timbers can be accurately monitored on micro-samples using a specialised experimental device developed by AgroParisTech – ENGREF. The device generated shrinkage data that varied between species but were consistent (repeatable) within a species. Collapse shrinkage was clearly evident with this method for *Eucalyptus obliqua*, but not with other species, consistent with industrial seasoning experience. To characterise the wood-water relations of this species, free of collapse, thinner sample sections (in the R-T plane) should be used.

Table of Contents

List of Abbreviations

2D	Two-dimensional
3D	Three-dimensional
AS/NZS	Australian and New Zealand Standard
A_i	Image area
A_{vj}	Lumen area
A_w	Wood tissue area
cos	Cosine
DETA	Dielectric thermal analysis
DMA	Dynamic mechanical analysis
DPI&F	Department of Primary Industries and Fisheries
DTA	Differential thermal analysis
E	Modulus of elasticity
ENGREF	l'École Nationale du Génie Rural des Eaux des Forêts
ENSIA	Ecole Nationale Supérieure des Industries Agricoles et Alimentaires
ESALQ	Escola Superior de Agricultura "Luiz de Queiroz"
ESEM	Environmental scanning electron microscope
E*	Complex modulus
E'	Storage modulus
E"	Loss modulus
F_c	Clamping factor
FCBA	Institut Technoligique Organisation Pôles et Stations
FE	Finite element
f_p	Fibre porosity
FSP	Fibre saturation point
FWPA	Forest and Wood Products Australia
G	Guaiacyl
H	Para-hydroxyphenyl
Hz	Hertz
H_2O	Water
INAP – G	Institut National Agronomique Paris-Grignon
INRA	French National Institute for Agricultural Research
IR	Infra-red
kg	Kilogram
L	Longitudinal or sample length

Lat.	Latitude
LERMAB	Laboratoire d'Etudes et de Recherche sur le Matériau Bois
I	Moment of inertia
IP	Intersection point
K_s	Stiffness
l_{fi}	Fibre lumen contour length
l_{lj}	Manually drawn contour length
L	Sample length
Long.	Longitude
M	Meter
MC	Moisture content
M_d	Oven dry mass
mm	Milimeter
MOR	Modulus of rupture
nm	Nanometer
NMR	Nuclear magnetic resonance
P	Applied force
PID	Proportional-intergral-differential
PC	Personal computer
PS	Polystyrene
PVC	Polyvinyl chloride
QUT	Queensland University of Technology
R	Radial
S	Syringyl
sin	Sine
S_1	First cell wall layer
S_2	Second cell wall layer
S_3	Third cell wall layer
T	Tangential
t	Time or sample thickness
tan	Tangent
t_{ave}	Average cell wall thickness
TG	Glass transition temperature
USA	United States of America
V_g	Green volume
w	Sample width
X	Magnification

ε_x	Strain
ε'	Dielectric permittivity
ε''	Dielectric factor
δ	Phase angle
δ	Amplitude of deformation
μm	Micrometer
v	Poisson's ratio
ρ_b	Basic density
σ_x	Stress
σ^*	Complex stress
σ'	Elastic stress
σ''	Viscous stress
°	Degrees
℃	Degrees Celsius
%	Percent

Chapter 1 - Introduction and Background

Timber drying depends on many different parameters. In general, practical objectives are related to low drying cost, short drying time and reasonable drying quality. To achieve an overall acceptable result of these mutually interfering targets, compromises are required. The complex system of intricate physical and mechanical processes during timber drying includes external heat and mass flow, coupled heat and mass transfer within wood, shrinkage induced stress deformation, and the mechanical memory behaviour of wood. Additional effects include chemical alterations leading to discolorations and physical phenomena, such as cell collapse.

Conventional kiln drying with controlled heating, humidity and air-flow under atmospheric pressure conditions is the primary method for drying timber in Australia (Nolan et al. 2003). In recent years, with emerging technological advancements in construction, computer control and less expensive materials, vacuum drying of hardwood timber has been proven (particularly in Europe and USA) in many applications to be a more economic alternative to drying using conventional methods, with similar or better quality outcomes (Savard et al. 2004). For this reason, the Department of Primary Industries & Fisheries (DPI&F) expanded its seasoning R&D capacity through the purchase of a 2 m^3 research vacuum kiln to investigate the viability of vacuum drying technology for drying Australian hardwood species. Initial kiln trials drying native forest *Corymbia citriodora* (spotted gum) and young plantation *Eucalyptus cloeziana* (Gympie messmate) have proven that these species can be vacuum dried approximately 60% faster than conventional drying, within acceptable grade quality limits (Redman 2006, Redman and McGavin 2008).

The results obtained from these preliminary vacuum drying trials generated much interest from the Australian hardwood timber industry. In response, Forest and Wood Products Australia (FWPA) in conjunction with various industry partners and DPI&F invested in a three year project (PN 08.2047) to establish the viability of vacuum drying technology for drying four high commercial volume Australian hardwood species in terms of drying quality, time and cost. Moreover, it was recognised that a better knowledge of the material and associated drying behaviour is required to fully optimise the vacuum drying process in the future. Therefore, the development of a hardwood vacuum drying model is included in the project.

Currently, much modelling work has been conducted for softwood species due to its commercial importance and relative homogeneity between species. The increased complexity of the wood structure of hardwoods together with the huge variation within and between species, have resulted in limited deterministic modelling work being performed to date on these species. Moreover, hardwoods often display complex mechanical and physical behaviours leading to specific forms of degrade phenomena such as cell collapse and internal checking (splitting) which are rarely a problem when drying softwoods. Some Australian hardwood eucalyptus species can be easily dried whereas other species of high commercial value are considered to be some of the most difficult to dry in the world (Vermaas 1995).

Over the past two decades the research team at ENGREF, Nancy France, led by Professor Patrick Perré have pioneered the development of fundamental wood drying research ranging from the kiln scale to the complicated transport phenomena evolving at the macroscopic and microscopic scales within the product. Research has included modelling of the coupled heat and mass transfer phenomena of anisotropic and heterogeneous media (i.e. wood) in both 2D and 3D (Perré and Turner, 1999a and 1999b) which has led to the subsequent development of a graphical user interface program known as *TransPore*. More recently *TransPore* has been updated to include a true dual scale approach, capable of dealing with wood variability and stack effect (Perré and Remond, 2007 and Perré, 2008). For the first time, a versatile computational tool based on high level scientific knowledge, capable of prediction, can be used to improve existing processes or develop new drying processes. The knowledge gained from this fundamental work has led to a better understanding of the drying process enabling the development of optimised drying systems and practice by drying practitioners worldwide. Mathematical modelling has been and still remains an integral component of research work at ENGREF.

As these models are based on a comprehensive set of macroscopic equations, they require a full set of physical and mechanical parameters. Consequently, the ENGREF laboratory has been set-up over a period of many years to characterise different basic properties of porous media. Special attention has been give to the wood properties which determine drying behaviour, such as density, permeability, capillary pressure, mass diffusivity, and mechanical and viscoelastic characteristics. This required the development of special experimental tools, such as a sensor to measure temperature and pressure simultaneously in wood during drying, the determination of MC profile using X-ray attenuation, a custom device able to measure the viscoelastic properties of wood under saturated conditions up to 140 °C (Placet et. al., 2008) and a device to accurately determine the wood-water relations on micro-samples (Perré, 2007).

Scaling in porous media is a new technique used by the ENGREF team to predict the macroscopic properties from morphological information of heterogeneous medium. This field involves characterisation at the microscopic scale, mathematical formulation, description of the medium structure, prediction of the macroscopic behaviour and validation. Excellent results have been obtained to predict shrinkage, elastic properties and some transfer properties of wood from its cellular structure (Badel and Perré, 2007). An environmental electron scanning microscope (ESEM) has recently been installed in the laboratory. This in conjunction with the software program *MeshPore*, developed by Perré (2005), has allowed intricate characterisation of wood at the cell wall level to be achieved. *MeshPore* is a standalone application allowing a comprehensive Finite Element (FE) mesh to be prepared from digital microscopic images of heterogeneous and porous media. Additionally, fast measurements of the wood morphology can be easily calculated, including cell wall thickness, porosity and cell dimensions.

As drying models require a number of physical and mechanical parameters to operate, appropriate initial parameters have been chosen for this fellowship, to gain a better understanding of the wood properties that explain the drying behaviour of Australian hardwood species and satisfy major requirements for the drying model of FWPA project PN08.2047. The

parameters chosen were prioritised for this fellowship as their measurement requires specialised tools and skills currently unavailable in Australia.

The following parameters were measured and are presented in this report, for *Corymbia citriodora* (spotted gum), *Eucalyptus pilularis* (blackbutt), *Eucalyptus marginata* (jarrah) and *Eucalyptus obliqua* (messmate):

1. measurement of wood anatomy characteristics using a combination of ESEM (environmental scanning electron microscope) scans and image analysis using *MeshPore* to characterise cell morphology;

2. measurement of the viscoelastic nature in the tangential and radial directions using dynamic mechanical analysis (DMA) and;

3. measurement of the wood-water relationship on micro samples using a highly accurate microbalance and laser technology to accurately measure loss of moisture content in conjunction with directional shrinkage.

1.1 Research Location

Research was conducted at AgroParisTech – ENGREF, Nancy campus, France. AgroParisTech was founded on January 1st 2007 by the three following graduate institutes in science and engineering:

INAP-G - Institut National Agronomique Paris-Grignon,

ENGREF - Ecole Nationale du Génie Rural, des Eaux et des Forêts and,

ENSIA - Ecole Nationale Supérieure des Industries Agricoles et Alimentaires.

AgroParisTech is a member of ParisTech, the Paris Institute of Technology, which is a consortium of 10 of the foremost French graduate institutes in science and engineering. AgroParisTech fosters strong international relationships which include: 100 partnerships with foreign universities, foreign students, representing 20% of the student body and, 3 students out of 4 spending a 2-month to 1-year period abroad.

The internal institute, ENGREF, is the national school of the agricultural engineering of water and forests. It is a multidisciplinary research institute specialising in forests and water research employing research scientists from biological, mathematics, physics and engineering disciplines. The research includes environmental management training, agricultural engineering of water and forests, management of public policies, management of water and waste, and environmental planning. ENGREF is established on several sites: four located in Metropolitan France (Nancy, Montpellier, Clermon-Ferrard), and one overseas in Kourou, French Guinea.

Research activities at ENGREF in Nancy (Figure 1 and Plate 1) concentrate on forests, wood and the management of natural environments. The centre consists of three research departments:

1. Department of Science and Engineering for Agronomy, Forestry, Water and the Environment.
2. Department of Science and Procedures for Food and Bio-products.
3. Department of Science and Economics for Social and Policy Management.

This research was conducted within the Department of Science for Food and Bio-products whose research areas include relations between the structure, the properties and the uses of wood and materials containing wood or fibres, modelling of the properties of wood, and, methodology for the development of industrial processes.

Figure 1. Project location, Nancy France (source: www.lonelyplanet.com).

Plate 1. ENGREF, Nancy (Lat. 48.6943, Long. 6.1895).

1.2 Wood structure

Before approaching the concepts governing the rheological and morphological behaviour of wood, it is necessary to have an understanding of wood structure. As the research presented in this report is concerned only with Australian hardwood species (angiosperms), the information described in this section covers only hardwood structure. The following information was obtained and summarised from Siau (1984), Ressel (2008), Bootle (2005) and Butterfield (1980).

1.2.1 Physical Structure

The physical structure of wood is non homogeneous by nature. This is reflected in timber properties such as density, moisture content and its general physical appearance. A mature tree is comprised of three main elements, namely, the crown or leaf system, the trunk or bole, and the root system.

The root system acts as an anchor for the tree as well as absorbing water and essential minerals from the soil.

The function of the tree crown is to manufacture food materials essential for tree growth. The leaves of a tree contain a green substance called chlorophyll which, with the action of sunlight, breaks down carbon dioxide. The oxygen is released back into the air through the leaves while the carbon combines with minerals and water absorbed by the root system to form food substances.

The trunk of a tree is the most important element with regards to this research and is the section from which commercially available timber is derived. The trunk of a tree is made up of several different layers. From the outer circumference of the trunk to the centre they are; the outer bark, inner bark, cambium layer, sapwood and heartwood.

The outer bark of the trunk is all dead tissue. It contains breathing pores known as lenticels which allow the flow of oxygen into the living tissue of the tree and the disposal of carbon dioxide into the atmosphere. The main purpose of the outer bark is to armour the tree and reduce water loss through evaporation.

The inner bark of a tree consists of thin, green, moist tissue which conducts food manufactured in the crown of the tree to the cambium layer.

The cambium layer consists of a very thin layer of cells that are responsible for all growth in trunk diameter. Growth takes place through the division of cells. The cambium layer forms new sapwood or xylem on the inside of the cambium and new inner bark or phloem on the outside. A new sapwood cell is laid down at a particular distance from the ground and retains that position for the life of the tree, therefore inner bark cells are formed outward from the tree centre as the tree grows.

The sapwood is the newly formed wood that surrounds the heartwood. It is composed of living cells whose function is to conduct water and minerals from the roots to the leaves. The sapwood is usually lighter in colour than the heartwood. The inner sapwood gradually hardens and turns into heartwood as the tree grows.

The heartwood is the fully matured part of the tree. The transition to heartwood is marked by the deposition of extractives and other extraneous material in the cells, and in the case of most eucalypt species, by the accelerated production of tyloses. Tyloses are cellular membranes which enter vessels (1.2.2.2) from adjacent parenchyma cells (1.2.2.3) through pit pairs and greatly increase the resistance of water flow through the heartwood. The death of the living cells then follows so that the heartwood is physiologically dead tissue. Its main function is to provide stability to support the tree.

Most woody plants from temperate climates exhibit light and dark rings through the cross section of the trunk between the cambium layer and the inner pith. These growth rings are produced as trees grow periodically rather than continuously. Growth rings are usually associated with seasonal changes or dramatic climate fluctuations. Generally the lighter growth rings are associated with rapid spring and early summer growth. This is called the earlywood and is softer and has large thin-walled cells compared to the darker latewood growth rings. Latewood is usually associated with slower growth in late summer and autumn. It consists of wood made up of cells comparatively narrower in width with thicker, stronger walls. The demarcation of growth rings in relation to seasonal effects is less pronounced and sometimes non-existent for subtropical and tropical wood species, compared with temperature species, due to less climatic variation between seasons.

1.2.2 Cell Structure

The basic cell structure of hardwoods consists of three cell formations produced on the inside of the cambium layer (xylem). These are the parenchyma cell (axial and ray), fibre and the vessel. Figure 2 shows a typical hardwood block magnified to $\times$ 250 with the various cell orientations and relative sizes shown. The LRT key represents the directions of the longitudinal, radial and tangential directions respectively.

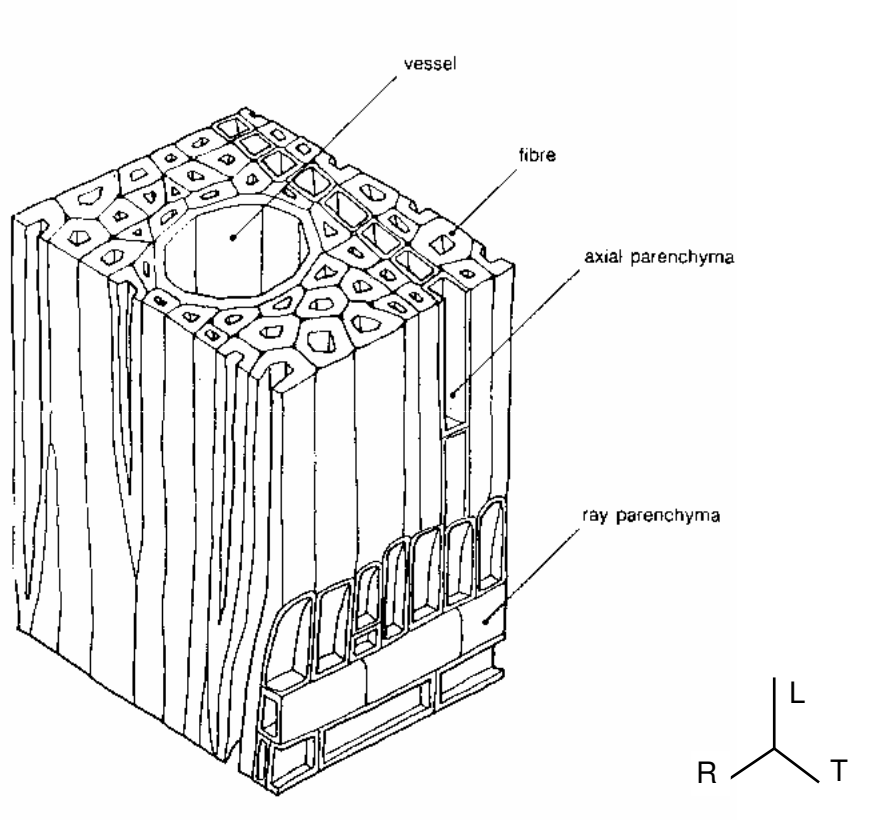

Figure 2. - Diagram of a hardwood cube (magnification × 250), cell pits have been omitted. Diagram extracted from Butterfield and Meylan (1980).

1.2.2.1 Fibres

Fibres make up the bulk volume of most hardwoods. Their primary role is to provide mechanical support for the tree. They are axially elongated cells that taper at each end to a point with generally a smaller mid-diameter than the other cell types. Their secondary walls are usually sparsely pitted and considerably thicker than those of the vessel elements and axial and ray parenchyma cells. Normally they have no living contents at maturity. The proportion of fibres present, fibre diameter, and the average thickness of their cell walls largely govern the density of a hardwood. Fibres overlap longitudinally and the lumens of adjacent fibres are connected by pits. Although pits are present in fibres of most eucalypt species, they are filled or occluded with various extractives.

1.2.2.2 Vessels

Hardwoods are sometimes called *porous woods* because of the vessels or 'pores' that are sometimes visible to the naked eye in clean cut transverse faces. The vessels perform the major water carrying functions in the living tree. The grouping of vessels and their mid-diameter varies considerably from one species to another. The diameter of the vessels of any given

species varies within each growth increment. Vessels, built up of individual vessel elements joined end to end provide a pathway for the conduction of water and dissolved mineral salts from the roots to the leaves.

Material moving through vessels passes relatively freely between individual 'end to end' cell elements through perforations in their walls. Perforations are virtually unobstructed openings in the end walls forming *perforation plates*. Extensive inter-vessel pitting is also present between vessel walls.

1.2.2.3 Parenchyma Cells

Parenchyma cells have thin walls with numerous pits and are generally brick shaped. They act as a form of storage tissue and are scattered in strands, patches or bands amongst the vessels and fibres. Unlike other wood cells, parenchyma cells remain alive for some years after completion of their development. Ray parenchyma is present in horizontal bands called medullary rays that radiate from the pith towards the bark.

1.2.3 Chemical Composition

Apart from extractives, wood cells consist primarily of three substances, cellulose, lignin and hemicellulose. Carbon dioxide from the atmosphere is combined with water obtained from the roots to photosynthesize simple sugars. When these sugars are conveyed from the leaves to the wood cells, they are changed into more complex cellulose, hemicellulose and lignin.

Cellulose consists of thousands of glucose molecular units chained together end to end to form polymers of simple sugars called polysaccharides. Cellulose exists in both crystalline and non-crystalline (amorphous) states. The percentage of cellulose present in wood is reported by Siau (1984) to be remarkably constant, namely 42% ± 2% in both softwoods and hardwoods. Crystalline cellulose is impermeable to water and it is only in the amorphous regions of the cell wall that water molecules become strongly bonded to the hydroxyl groups of cellulose. Thus, cellulose contributes to the water absorption of wood through its numerous hydroxyl groups.

Hemicelluloses like celluloses are polysaccharides. They are associated with cellulose and lignin in the cell wall and are gelatinous by nature. The major hemicellulose in hardwoods is an acidic xylan and accounts for 25% ± 5% of the extractive free wood (Siau 1984).

Lignins are three dimensional polymers composed primarily of phenylpropane units and have a relatively high molecular weight compared with cellulose and hemicellulose. Siau (1984) reports that the cell wall material (not including water) of temperate hardwoods is comprised of 25% ± 3% lignin. Lignin offers protection to the wood against microbial degradation and it also serves to reduce its hygroscopicity. Cellulose and especially hemicellulose are far more hygroscopic than lignin.

Lignin is categorised into three types: guaiacyl (G), syringyl (S) and para-hydroxyphenyl (H). It is well known that the G, S and H ratio of lignin in softwoods (gymnosperms) and hardwoods (angiosperms) are different. A large variability of SG lignin ratio exists in hardwoods. The hardwood SG ratio varies between 20 and 60% and is influenced by species, age, and position within the tree. Studies have shown that the viscoelastic softening temperature (discussed in detail in section 1.3) TG is influenced by the SG ratio of lignin. A high SG ratio, or high S content results in a lower softening temperature (Placet 2006).

1.2.4 Cell Wall Structure

Wood cell walls consist of the three major components mentioned above where cellulose is the skeleton, hemicellulose is the matrix and lignin is the adhesive substance binding the cells together and giving rigidity to the cell wall.

Cellulose polysaccharides in woody plant cells are chained together to form extremely long crystalline microfibrils of great tensile strength. These microfibrils are embedded in and coated by the lignin and hemicellulose to form a matrix. Thus the wall structure forms a natural fibre-composite. This differs from most artificial composite materials in that the matrix is water reactive and changes both its volume and elastic properties with moisture content.

Wood cell walls consist of a primary wall and secondary wall. The primary wall is the first to develop and is stretched and elongated during initial growth of the cell. It consists of a thin network of randomly arranged microfibrils and is only 0.1 to 0.2μm thick (Siau 1984). The primary wall is the only wall present in parenchyma cells (see section 1.1.2.3). The secondary wall is then laid down on the inside of the primary wall, usually after elongation of the cell has ceased.

The secondary wall is further subdivided into three layers designated S_1, S_2 and S_3, each having different helical arrangement of its microfibrils. The following values of layer thickness and microfibril angle are from Siau (1984). The layer nearest the primary wall is called the S_1 layer. The S_1 layer is 0.2 to 0.5 μm thick in earlywood and can reach a thickness of 1 μm in latewood. The microfibrils of the S_1 layer are orientated at an average angle of 60° to 80° to the fibre axis.

The middle or S_2 layer is the thickest of the three secondary wall layers with thickness from 1.0 to 2.0 μm in earlywood and from 3 to 8 μm in latewood. The microfibril angle of this layer also varies between the earlywood and latewood from 10° to 30° to the fibre axis respectively.

The S_3 layer, lying nearest to the cell cavity or lumen, is only 0.1 to 0.2 μm thick in both earlywood and latewood. Its microfibrils are almost transverse to the fibre axis.

Individual cells are joined together by intercellular material between their primary walls called the middle lamella. The middle lamella is an amorphous mass, rich in lignin and low in cellulose. When the formation of the cell is complete, impregnation of the middle lamella with lignin begins, and gradually extends throughout the cell wall. The many capillaries present

between the microfibrils become filled with polyphenols and other extractives when the sapwood changes into heartwood.

The following diagram illustrates the general structure of the wood cell wall and the helical orientation of the cellulose microfibrils within each wall layer.

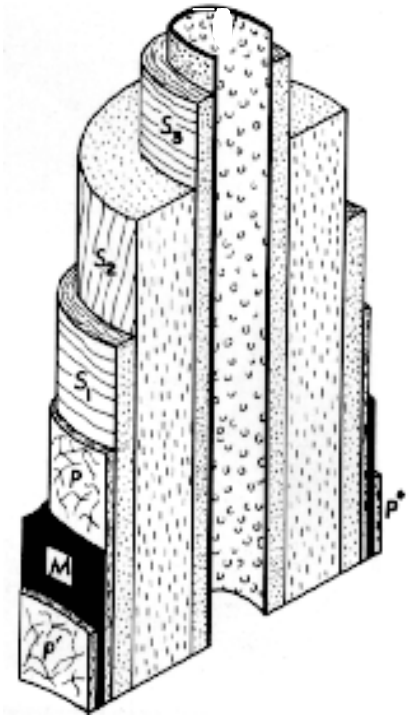

Figure 3 - A diagram illustrating the general structure of the cell wall of axially elongated wood elements and the helical orientation of the cellulose microfibrils within each wall layer. M, middle lamella; P, primary wall; S_1, outer layer of the secondary wall; S_2, middle layer of the secondary wall; S_3, innermost layer of the secondary wall; P', primary walls of adjoining cells. Diagram extracted from Siau (1984).

During the cell formation process there are regions in the secondary cell wall, which develop and are known as *pits*. Pits form a canal between the cell lumen and the primary wall which permits the flow of liquid from one cell to another. The pits of two adjoining cells usually oppose one another to form a *pit-pair*. The primary walls of the two such opposing cells, and the intervening middle lamella, form what is termed the *pit membrane*. In softwoods, open pits allow free and relatively rapid flow of water, however for Australian eucalypts, pit openings are very small and often occluded so that water movement is dominated by molecular diffusion (Cronshaw 1960).

1.2.5 Wood and water

Wood is a hygroscopic material. Its water content changes/moves according to the percentage of moisture of the ambient air which it is in contact. Wood can contain water in two forms: free water and bound water. Free water fills the cellular lumens and is retained within wood by mechanisms of capillary pressure. The macromolecular structure and in particular the hydroxyl groups of polysaccharides are strongly absorbent and can accommodate water molecules bound by weak Van der Waals bonds. During wood drying water migrates either, freely as a fluid (liquid and/or gas) between and within wood cells via capillary migration, or as water or vapour diffusion between the macromolecular structure (Skaar, 1988).

1.3 Viscoelastic Behaviour of Wood

Viscoelasticity is the study of materials that exhibit both viscous and elastic characteristics when undergoing deformation. Viscous materials, like honey, resist shear flow and strain linearly with time when a stress is applied. Elastic materials strain instantaneously when stretched just as quickly in return to their original state once the stress is removed. Viscoelastic materials have elements of both of these properties and, as such, exhibit time dependent strain. Whereas elasticity is usually the result of bond stretching along crystallographic planes in an ordered solid, viscoelasticity is the result of the diffusion of atoms or molecules inside an amorphous material.

Wood is classed as a viscoelastic material and the majority of the mechanical properties of wood depend closely on its hygrothermic state. For example, hot and wet wood is malleable and can be easily reformed. When it is subsequently cooled and dried, it solidifies its form. This characteristic is exploited industrially and is the principle of thermoforming, bending and veneer peeling. The rheological[1] property at the origin of this behaviour is the viscoelasticity of wood. Viscoelasticity is a characteristic of polymers behaviour between that of an elastic solid and that of a viscous fluid. Wood material is made up of a mixture of three polymers: the cellulose hemicellulose and lignins. The polymers are also distinguished from other materials by their glass transition temperature TG. The glass transition temperature marks the border between two fundamental states: the elastic state and the plastic state.

This temperature of softening, where wood becomes malleable, makes it possible to optimise steam bending and can also be critical in other processes such as drying and veneer peeling or slicing. A strategic use of the viscoelastic properties of wood makes it possible to accelerate the process of drying (Aguiar and Perré, 2000). It is possible to decrease the constraints of drying wet wood (above fibre saturation point) by drying at the glass transition temperature. Moreover, the viscoelastic properties of wood and in particular the glass transition temperature depend closely on the anatomical and biochemical structure of wood. The characterisation and the modelling of the viscoelastic behaviour of wood are thus crucial to optimise and simulate industrial processes.

[1] Rhelogy is the study of the deformation and flow of matter under the influence of stress.

1.3.1 General characteristics of polymers

A polymer can be of natural origin (i.e. rubber, cellulose, and collagen) or chemically synthesised via a polymerisation reaction (i.e. PVC: polyvinyl chloride, PS: polystyrene). A polymer is a material made up of long molecular chains called macromolecules. They consist of a principal chain, also called a skeleton, on which atoms of different chemical nature or molecules (i.e. H_2O) can be laterally substituted. These groups of atoms are called substituents. They can either stabilise and rigidify or weaken the macromolecule. The primary bonds (covalent) are of a chemical nature. They ensure a strong energy bond between the monomeric units (40-800 KJ/mol). The secondary connections ensure cohesion between macromolecules via physical forces of cohesion. The binding energy is roughly from 2 – 20 KJ/mol (Ehrenstein and Montague 2000).

The TG of a polymer is directly related to the mobility of molecular groups or sequences within the polymer and sliding movement of polymeric chains. At low temperature, the molecules have minimal mobility. When the temperature is raised, the molecules receive a thermal energy contribution and become more mobile due to thermal agitation. Many parameters may affect a polymers glass transition temperature. However, the parameters having the greatest influence are related to the flexibility of the macromolecular chains, the size and polarity of the side groups and the molecular mass (Placet 2006).

1.3.2 Techniques to measure viscoelastic properties

The particular structure of polymers makes it possible to measure a number of properties such as thermal, magnetic, electric, mechanical etc. The transitory properties are often characterised by a sharp variation in these properties. Numerous methods are available to characterise and study the phenomena of polymer transition.

The earliest method to determine the glass transition of a polymeric material consisted of measuring the variation of specific volume or dimensions of a sample according to the temperature. Although this testing method is relatively simple, the accuracy is doubtful as TG obtained in this manner changes depending on the heating/cooling speed of the sample.

The measurement of the heat-storage capacity is an excellent indicator of a polymer's TG. This technique is called Differential Thermal Analysis (DTA) and was developed in 1899 by Roberts-Austen (Placet, 2000). In DTA, the temperature variation is measured between a sample and an inert material of reference placed in an environment whose temperature increases at programmed constant speed. A transition results in a displacement of the measurements, proportional to the increase in heat-storage capacity of the sample. However, similar to the specific volume method, the glass transition temperature measured by DTA is dependant on the heating/cooling speed.

Viscoelasticity can be measured using IR (infra-red) and NMR (nuclear magnetic resonance) techniques. These methods consist of exciting samples at certain frequencies and studying the behaviour of the molecules and atoms of a material. These spectroscopic methods are very

powerful, however their disadvantage lies primarily in the cost and also that they do not make it possible to directly determine the values of the viscoelastic properties.

A recent method to quantify viscoelasticity is by Dielectric Thermal Analysis (DETA). This is an oscillatory method where an electric field of weak voltages is applied to the sample. The complex permittivity[2] can be determined by measuring the variations of amplitude and phase of the return electric current. The complex permittivity can be divided into the dielectric permittivity (ε') which represents stored electrical energy and in the dielectric factor (ε") which represents the energy dissipated in the material. TG results in the zone where the value of ε"/ε' is maximum.

The most widely used method to characterise the viscoelastic nature of materials is via mechanical testing techniques. This method of test can be split into two types: quasi-static and harmonic tests. Quasi-static test methods consist of recording curves of restraint or deformation during time. The most common tests are creep tests. During creep tests a constant force is applied to a sample and the deformation is measured over time. This test can be performed under changing thermal conditions. The disadvantage with thermally activated creep tests is that the effects of time and temperature can not be uncoupled. This is not the case for harmonic viscoelastic tests, the method used for this research.

Harmonic tests consist of applying a forced vibration to a sample at a given frequency. The tests are generally categorised by the frequency band at which the vibrations take place. With very low frequency ($0 < f(t) \leq 1$ Hz) pendulums of torsion or deflection can be used. For low frequency tests (up to a few tens of Hz) excitation by alternate bending is usually employed. The technique is referred to as Dynamic Mechanical Analysis or DMA and many commercial apparatus are available to perform these tests. This type of instrument is able to apply various modes of deformation (deflection, compression, tension, shearing etc.) and allows the evolution of viscoelastic properties according to the constraint, frequency and temperature. These apparatus provide powerful and practical measurements of viscoelasticity as tests can be made at varying frequencies, displacements and temperatures in a relatively short time period. The DMA deflection test method was used to characterise the viscoelastic properties for this research (explained further in section 1.3.3).

[2] Permittivity relates to a materials ability to transmit (or permit) an electric field.

1.3.3 Dynamic mechanical analysis - DMA

The concept of viscoelasticity comes from the fact that most materials do not exhibit purely elastic (ideal solids) or purely viscous (ideal liquids) behavior but a combination of both. When a stress is applied to a viscoelastic material, it will show time-dependent deformation. Any viscoelastic material, given enough time, will flow under an applied stress. When the stress is removed the material will not fully recover. The portion of strain that is recovered represents the energy stored or the elastic portion of the material's response. The portion of the strain that is not recovered represents the energy dissipated or viscous portion of the material's response.

Dynamic Mechanical Analysis (DMA) is a technique used to measure the mechanical properties of a wide range of materials. DMA measures the viscoelastic properties using either transient or dynamic oscillatory tests. The most common test is the dynamic oscillatory test. During dynamic testing, an oscillatory (sinusoidal) strain (or stress) is applied to the material and the resulting stress (or strain) developed in the material is measured. For an ideal solid material, which obeys Hooke's law, the resulting stress will be proportional to the amplitude of the applied strain. The stress and strain waves will be in phase or, put another way, the phase shift (phase angle δ) between the stress and strain is 0° (Figure 4). For an ideal fluid which obeys Newton's law, the stress will be proportional to the strain rate. The stress signal will lead the strain signal by 90° (Figure 4). For a viscoelastic material, the phase angle will lie somewhere between 0° and 90° (Figure 5).

As the *modulus* is defined as the ratio of stress to strain (stress/strain), the resultant stress generated in a viscoelastic material, also referred to as the *complex stress* (σ^*), can be used to calculate the *complex modulus* (E^*). The complex modulus is a measure of the materials resistance to deformation. It encompasses both elastic and viscous responses. The power of dynamic oscillatory testing is that, by using the measured phase angle, the stress in turn can be separated into two parts:

- an elastic stress (σ'), that is in phase with the strain, and
- a viscous stress (σ''), that is in phase with the strain rate (90° out of phase with the strain).

The elastic modulus, or *storage modulus* (E') and the viscous modulus, or *loss modulus* (E''), can then be calculated directly from the elastic and viscous stress respectively. A summary of the calculations are as follows:

Complex Modulus

$$E^* = \sigma^*/\varepsilon \qquad \text{or}$$

$$E^* = E' + iE^* \tag{1}$$

Storage Modulus

$$E' = \sigma'/\varepsilon \quad \text{or}$$

$$E' = E^* \cos \delta \qquad (2)$$

Loss Modulus

$$E'' = \sigma''/\varepsilon \quad \text{or}$$

$$E'' = E^* \sin \delta \qquad (3)$$

Figure 6 shows a vector depiction of these calculations. It can be seen from this figure that the tangent of the phase angle is the ratio of the loss modulus:

$$\tan \delta = E''/E' \qquad (4)$$

This ratio is the measure of the damping ability of a material and is used to determine the glass transition temperature TG. All of these parameters can be calculated as a function of time, temperature, frequency, or amplitude (stress or strain) depending on the application.

Because the TG has a kinetic component, it is strongly influenced by the frequency (rate) of deformation. As the frequency of the test increases, the molecular relaxations can only occur at higher temperatures and, as a consequence, the TG will increase with increasing frequency. In addition, the shape and intensity of the tan δ (TG) peak as well as the slope of the storage modulus in the transition region will be affected. Based on end-use conditions, it is important to understand the temperature and frequency dependence of transitions.

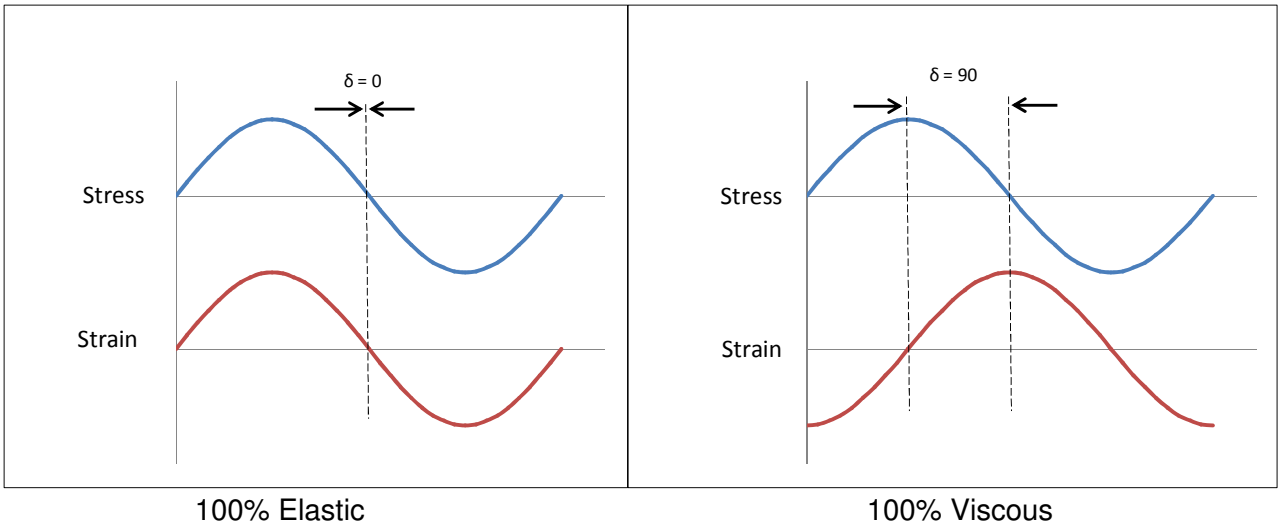

Figure 4. Ideal solid and fluid – DMA stress and strain.

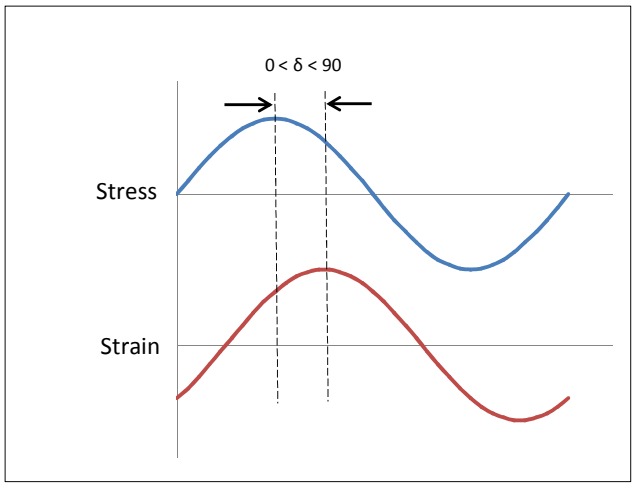

Figure 5. Viscoelastic material – DMA stress and strain.

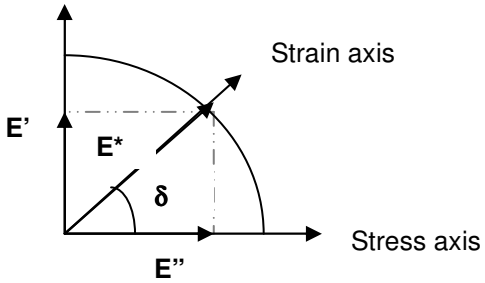

Figure 6. Complex plane representation of phase shift and modulus (E).

1.4 Wood-water relations – shrinkage and stress

To appreciate the fundamental phenomena of drying induced shrinkage and stress it is necessary to understand the relationship of each to the removal of water from wood. Green wood contains free water in the cell lumens and bound water in the cell wall. During drying, free water is generally removed before bound water. When the cell's lumens are empty of free water but all bound water remains, the wood is said to be at the fibre saturation point (FSP). The FSP is expressed as a percentage of moisture content (MC). Normal shrinkage occurs at MCs below FSP in all timbers due to the removal of bound water from cell walls. Conversely, swelling occurs at MCs up to FSP when adsorption takes place. The phenomena of shrinkage-swelling differs according to the material direction because of the strong anisotropy of wood.

The shrinkage of wood during drying is one of the most important properties as it is responsible for deformations during drying (twist, spring, bow and cupping), dimensional variations in situ, and is the driving force for stress. In turn, stress is responsible for most drying related defects including: surface and internal checking, end splitting, case hardening, and residual drying stress.

During wood drying, shrinkage starts once the outside layer reaches FSP. The core of the timber is still above fibre saturation point and consequently will not shrink. This creates a stress gradient within the timber, as the shrinking surface fibres go into tension, and the core, which is restraining the shrinkage, goes into compression. This sets up a shrinkage/stress gradient between the inner core of the timber and the outer shell. If the tensile force on the outer shell exceeds the modulus of rupture (MOR) the surface of the board will split or check. Once the core of the timber dries below fibre saturation point the stresses in the timber reverse, with the shell now restraining the core as it tries to shrink. The core then goes into tension and the shell into compression. This effect can cause internal checking and case hardening if the surface tension in the first part of drying was great enough to cause 'tension set'. Additionally, differential shrinkage caused by differences in radial, tangential, and longitudinal shrinkage is a major cause of distortion of timber during drying.

Chapter 2 – Morphological characterisation

2.1 Introduction

To obtain a better understanding of the wood drying process it is important to comprehend the anatomical features and its overall effect on drying. The work presented in this chapter identifies important anatomical characteristics and differences between the species investigated to characterise the cell morphology. The resulting data will provide the necessary cell morphology information to build a unit cell for further finite element meshing and subsequent modelling.

2.2 Materials and methods

2.2.1 Environmental Scanning electron microscope

An environmental scanning electron microscope (ESEM) is a type of electron microscope that images a sample surface by scanning it with a high-energy beam of electrons, usually under partial vacuum. The electrons interact with the atoms that make up the sample producing signals that contain information about the sample's surface topography, composition and other properties such as electrical conductivity. These signals are collected with appropriate detectors. The output of these detectors modulates, via appropriate electronics, the screen of a monitor to form a pixel by pixel image, emanating from the specimen surface.

An ESEM can produce very high-resolution images of a sample surface revealing details about 1 to 5 nm in size. Due to the way these images are created, SEM micrographs have a very large depth of field yielding a characteristic three-dimensional appearance useful for understanding the surface structure of a sample. A wide range of magnifications is possible, from about x 25 (about equivalent to that of a powerful hand-lens) to about x 250,000, about 250 times the magnification limit of the best optical microscopes.

The ESEM used for this research was a Quanta 200 3D manufactured by FEI[3] as shown in Figure 7. The microscope has a resolution of 3 nm and its main components consist of: a vacuum pump, electron emission column, sealed specimen chamber and image processing facilities.

[3] See http://www.fei.com/products/families/quanta-family.aspx for more infomation.

Figure 7. FEI Quanta 200 3D environmental electron scanning microscope.

2.2.3 Meshpore

Meshpore is a powerful software package used to apply image-based meshing techniques to anisotropic and heterogeneous porous media. This stand alone application allows a comprehensive finite element mesh to be prepared from digital images and can also be used to determine important morphological properties of porous media, such as average cell wall thickness and media porosity.

Using a number of mathematical algorithms the application is able to automatically describe cell contours by segment chains, allowing additional chains to be added, deleted, and altered. Once the media has been suitably described, *Meshpore* can generate a finite element mesh (as a file suitable for *EasyMesh*) useful for subsequent modelling tools such as *TransPore 2D* (Perré and Turner, 1999a).

2.2.3 Sample preparation

For each species, small heartwood samples were cut from unseasoned boards used for vacuum drying trials from FWPA project PN08.2047 - *Evaluation of super-heated steam vacuum drying viability and development of a predictive drying model for Australian commercial hardwood species*. One sample per species was carefully cut using a laboratory bandsaw to the approximate dimensions: 4 mm (radial) x 4 mm (tangential) x 20 mm (longitudinal). The samples were cut in half lengthwise to produce two matched samples of dimension: 4 mm x 4 mm x 10 mm. One section was used for ESEM analysis while the other section was used to determine basic density.

The ESEM samples were soaked in water at room temperature for at least 24 hours, before further processing, to soften the wood tissue prior to image surface preparation. One of the radial/tangential surfaces was prepared for ESEM imaging using a precision MICROM HM 440™ sledge/sliding microtome (Plate 2). This process provides a flat, sharply sliced surface essential for producing high quality ESEM images. Samples were loaded into the ESEM specimen chamber (Plate 3), levelled and scanned at 200 X 400 X and 800 X magnifications. Images at 800 X magnification were cropped to include only the wood fibres (not ray parenchyma or vessel cells) and analysed using *MeshPore* to determine the average fibre cell wall thickness and wood porosity.

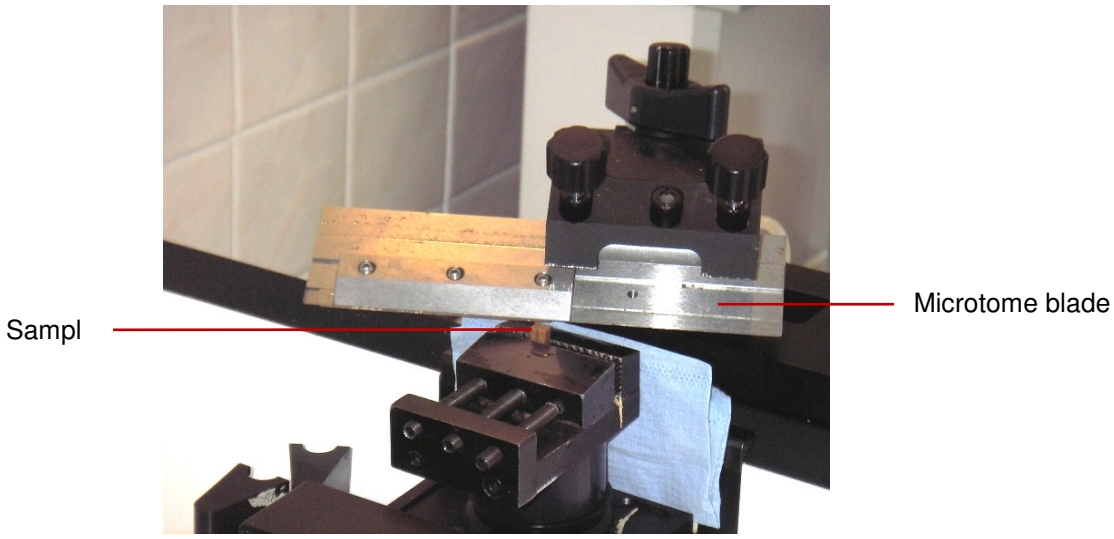

Plate 2. Sample surface preparation using a MICROM HM 440™ sliding microtome

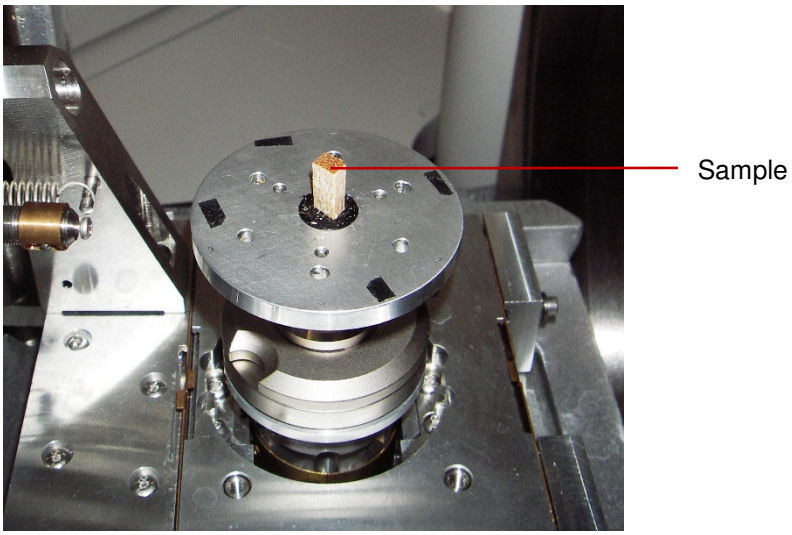

Plate 3. Sample placed in ESEM specimen chamber

Basic density was calculated by determining a samples green volume and dry weight in accordance with *Australian and New Zealand Standard AS/NZS 1080.3:2000 – Timber – Methods of Test – Method 3: Density* (Standards Australia 2000). To ensure samples were fully

saturated they were placed in a beaker of water, which was positioned in an airtight container surrounded by an ice/water mixture (Plate 4). The ice water was used to maintain the samples at low temperature to minimise leaching of extractives and provide accurate density measurements. The container was connected to a small vacuum pump and a vacuum pressure of 15 mbar was drawn. The samples remained in this state for approximately 1 hour before slow depressurisation. This was repeated 3 times to ensure the samples were fully saturated. The green volume of the samples was determined using the water immersion method. The samples were then dried in a laboratory oven at 103 ± 2℃ for 48 hours and weighed to determine the oven dry weight. Sample basic density was calculated using:

$$\rho_b = \frac{m_d}{V_g} \tag{5}$$

Where ρ_b is the basic density (kg/m^3), m_d is the oven dry mass (kg), and V_g is the green volume (m^3).

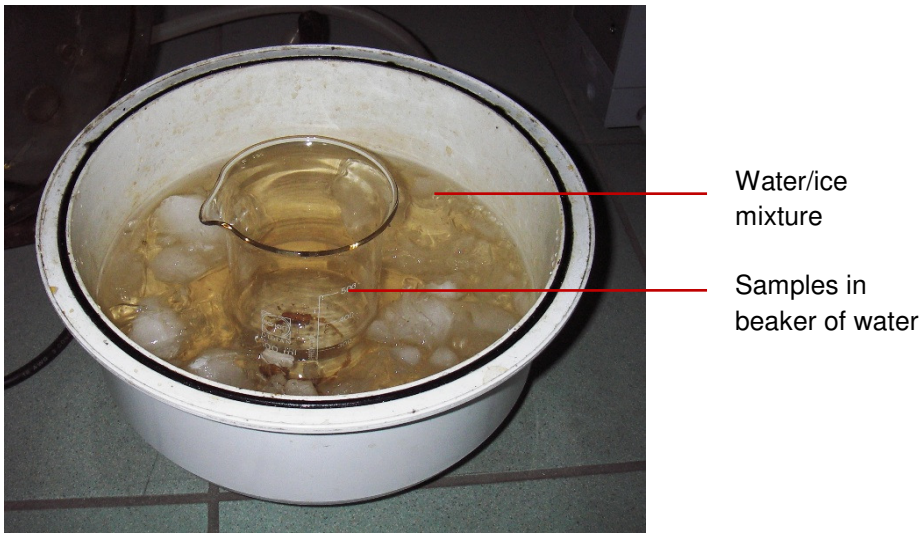

Plate 4. Samples prepared for vacuum saturation (container uncovered for photo)

2.3 Results and discussion

Appendix A contains the ESEM images for each species sample, taken at 200 X, 400 X and 800 X magnifications. Images taken at 800 X magnification were used for measurement of fibre properties using *Meshpore*. The ESEM images taken at this magnification were cropped to contain only wood fibre cells as shown in Figure 8. Ray parenchyma and vessel cells were excluded.

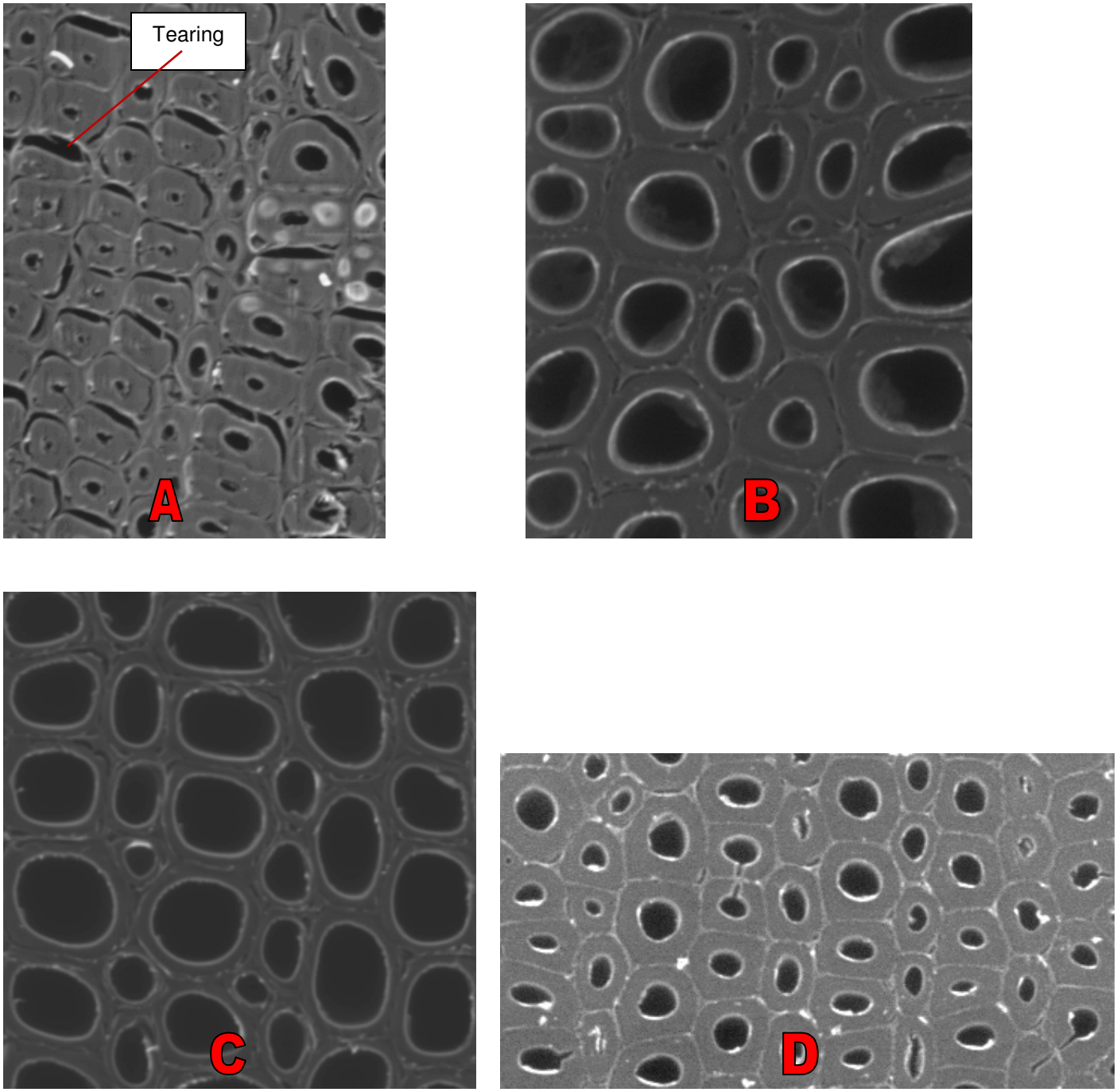

Figure 8. Cropped ESEM images for *Meshpore*: *Corymbia citriodora* (A), *Eucalyptus marginata* (B), *Eucalyptus pilularis* (C), *and Eucalyptus obliqua* (D).

A clear difference in fibre porosity, size, wall thickness and orientation is evident between species. For instance *Corymbia citriodora* is made up of fibres with very thick cell walls, and hence low porosity or lumen/wood tissue ratio, compared with *Eucalyptus marginata* whose fibres have large lumens and thin cell walls. Tearing of the middle lamella is evident for *Corymbia citriodora* (Figure 8). This was caused by the microtome blade during sample preparation. Due to the high density of this species it was extremely difficult to slice the surface to produce a quality image free of artefacts. Longer soaking times and boiling samples in water for 24 hours was trialled but with no improvement slicing and hence, image quality.

These images were loaded into the *Meshpore* software and contours of the cell lumens were automatically generated as shown in Figure 9 for *Eucalyptus pilularis.* From these contours, the fibre porosity is calculated by *Meshpore* using:

$$f_p = \frac{\sum_{i=1}^{n} A_{vj}}{A_i} \times 100 \qquad (6)$$

Where f_p is the fibre porosity (%), A_{vj} is the void (lumen) area (m^2) of lumen number j, n is the number of lumens in the image, and A_i is the area of the image (m^2).

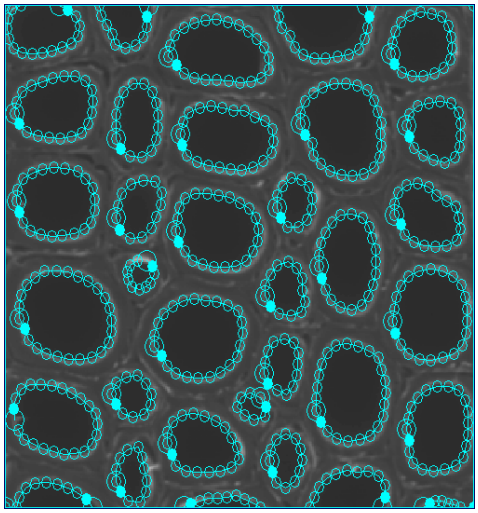

Figure 9. Automated Meshpore contour generated for *Eucalyptus pilularis*.

The average fibre cell wall thickness is calculated automatically by *Meshpore* using:

$$A_w = A_i - \sum_{i=1}^{n} A_{vj} \tag{7}$$

and

$$t_{ave} = \frac{A_w}{\sum_{j=1}^{n} l_{fj}} \tag{8}$$

Where A_w is the area of the wood tissue (m^2), t_{ave} is the average cell wall thickness (m) and l_{fj} is the length of fibre lumen contour (m) number j, n is the number of lumens in the image.

Average fibre thickness was also determined using a manual Meshpore method. Lines were manually drawn from the shortest point between adjacent cell wall/lumen interfaces as illustrated by Figure 10 for *Eucalyptus pilularis*. Using this method, the average cell wall thickness was calculated using:

$$t_{ave} = \frac{\sum_{j=1}^{n} l_{lj}}{2} \tag{9}$$

Where l_{lj} is the length of drawn line (m) number j, and n is the number of drawn lines.

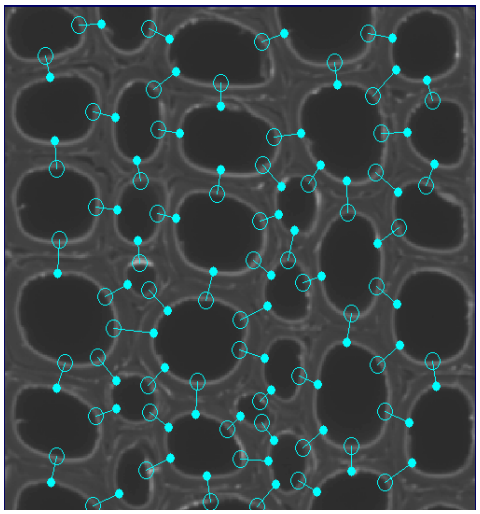

Figure 10. Manually drawn lines to determine average fibre wall thickness for *Eucalyptus pilularis*.

Table 1 contains the automatically and manually generated average fibre cell wall thickness, fibre porosity, and density for each species sample. Distinct fibre porosity and fibre cell wall thickness differences between species were measured, as visually observed from ESEM images. Large discrepancies exist between the automatic and manual generation of average fibre cell wall thickness. The automated calculations are subject to errors for wood cells with

very small lumens and thick cell walls, and cells that are irregular in shape as opposed to perfectly round cells, as they are heavily dependent on the length of lumen contours. This is evident when comparing the automatic and manually generated results for *Eucalyptus pilularis* (large lumens, thin cell walls) with *Corymbia citriodora* (small lumens, thick cell walls), whereby the discrepancy is exaggerated for the latter species. Tearing of the middle lamella of the *Corymbia citriodora* sample also contributed to cell wall thickness errors when using the automated method. Therefore, the manually generated fibre cell wall thickness values are considered the most accurate in this case as they are more consistent with published data. Ressel (2008) suggests the average fibre cell wall thickness for wood generally ranges from around 3 µm to 8 µm.

Except for *Eucalyptus obliqua*, density decreases with decreasing fibre cell wall thickness. Although fibre cell wall thickness plays an important role in the overall density of wood, the frequency and cell wall thickness of ray parenchyma cells, and the frequency and size of hardwood vessels also contribute (Ressel, 2008). These parameters are yet to be quantified.

Table 1 Average cell wall thickness, fibre porosity and density for each species

Species	Cell wall thickness (µm)		Fibre	Density
	Automatic	Manual	Porosity	(kg/m³)
C. maculata	16.4	5.4	5.4%	833
E. marginata	5.0	2.8	31.4%	721
E. pilularis	4.3	2.6	43.8%	681
E. obliqua	8.7	4.2	13.4%	418

2.4 Conclusions

- Morphological characterisation, in terms of fibre cell wall thickness and porosity, has been achieved for *Corymbia citriodora*, *Eucalyptus pilularis*, *Eucalyptus marginata* and *Eucalyptus obliqua*. A clear difference in fibre porosity, size, wall thickness and orientation is evident between these species.

- Considerable discrepancies exist between the automatic and manual generation of average fibre cell wall thickness, using *Meshpore*. This is exacerbated by irregular shaped fibres, wood with larger average fibre cell wall thicknesses and surface tearing caused by sample preparation. For these species, the more time consuming, manual method of fibre cell wall thickness determination was deemed more accurate when compared to published data.

- To fully characterise the cellular morphology of these species, additional work is required to investigate ray and vessel cell morphology.

2.5 Further work

Investigations of ray and vessel morphology for each species is planned to fully characterise the cellular morphology, allowing a unit cell to be derived for future modelling activities.

Chapter 3 – Viscoelastic characteristics using DMA

3.1 Introduction

The viscoelastic behaviour of wood is critical in many fields of the wood industry. It is especially important in wood processing operations such as drying, forming, steam bending, veneer processing and gluing. This behaviour depends on the wood species (Hamdan *et al.*, 2000), the type of wood (i.e. juvenile wood, sapwood and reaction wood (Lenth and Kamke, 2001), and the material direction (Placet *et al.*, 2008). Additionally, temperature and moisture content levels significantly affect the viscoelastic behaviour of wood (Irvine 1984).

Dynamic mechanical analysis (DMA), to characterise the viscoelastic properties of *Corymbia citriodora*, *Eucalyptus pilularis*, *Eucalyptus marginata*, and *Eucalyptus obliqua* is presented in this chapter. Results obtained for samples in radial and tangential directions are compared and discussed within and between species.

3.2 Materials and methods

3.2.3 Experimental device

Viscoelastic characterisation tests were performed using a TA Instruments DMA 2980 analyser. The instrument is made up of two main components: the DMA cabinet and DMA assembly. The DMA assembly is made up of the mechanical section enclosure, the sample clamp assembly, the furnace assembly (used to heat and cool the sample) and a high precision thermocouple. The DMA cabinet houses the instruments electronics. The display is used to monitor the instrument state and operating parameters (Plate 5). The entire viscoelastic analysis system consists of the DMA 2980 instrument, a PC utilising TA instruments controller and associated software, and an anti-vibratory table, to limit the disturbances due to external vibrations (Plate 6).

The DMA was developed by TA Instruments with the following features:

- operates over a temperature range of -145°C to 600°C, using heating rates up to 50°C/min,
- determines changes in sample properties resulting from changes in five experimental variables: temperature, time, frequency, force, and strain,
- uses samples that can be in bulk solid, film, fibre, gel, or viscous liquid form, and
- employs interchangeable clamps allowing measurements of many properties including: modulus, damping, creep, stress relaxation, glass transition, and softening point.

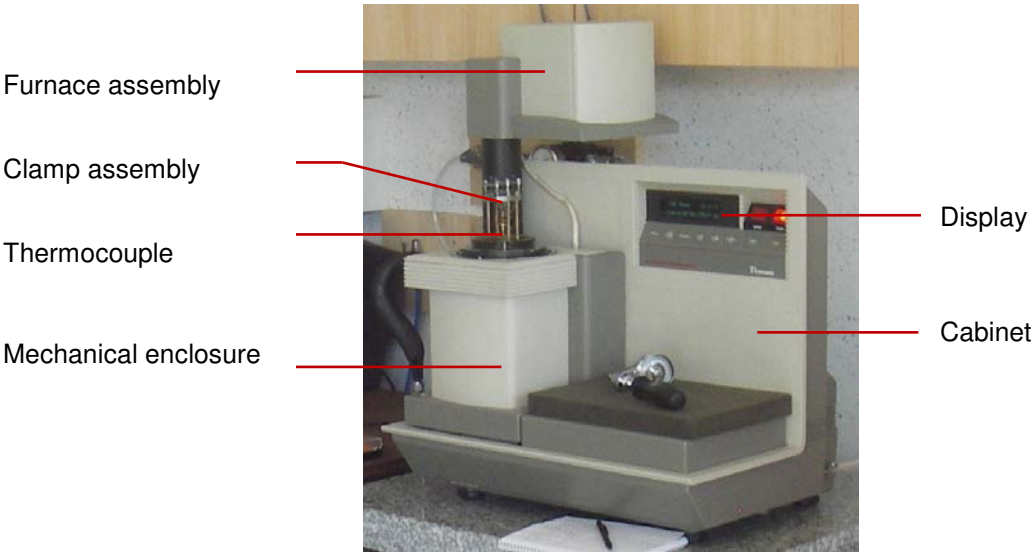

Plate 5. The DMA 2980 instrument.

Plate 6. DMA measurement system.

A single/dual cantilever clamp was used for the reported tests. In this mode, the sample is clamped at both ends and either flexed in the middle (dual cantilever) or at one end (single cantilever). Cantilever bending is a good general-purpose mode for evaluating thermoplastics and highly damped materials (e.g., wood). The single cantilever method was used for these tests as illustrated by Figure 11.

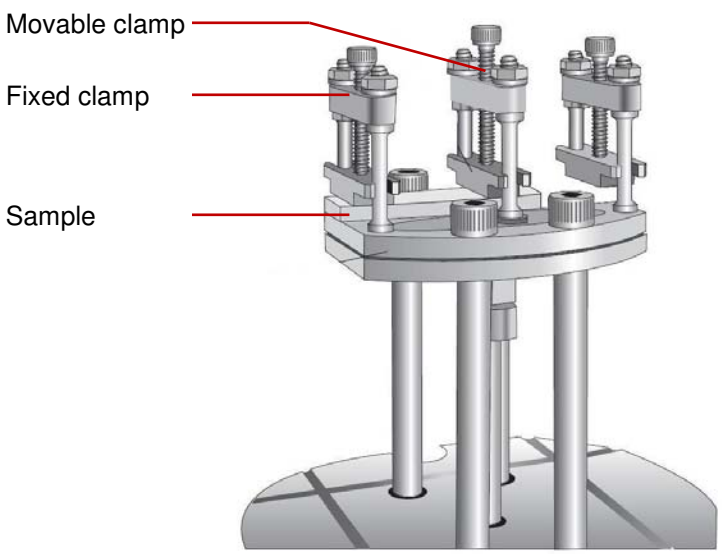

Figure 11. Dual/single cantilever clamp in single cantilever mode.

3.2.4 Single cantilever calculations

During operation, a sample is mounted on the clamp and then subjected to oscillatory changes in stress/strain while undergoing a change in temperature. The DMA measures the raw signals of force and amplitude of deformation. Stress and strain are derived from the raw force and amplitude, normalised for the geometry factor. This section provides the calculations used by the DMA 2980 software to calculate the modulus, stress and strain values.

The stiffness model equation for a rectangular cross section sample, analysed on the single cantilever clamp, is as follows:

$$E = \frac{K_s}{F_c} \cdot \frac{L^3}{12 \cdot I}\left[1 + \frac{12}{5} \cdot (1+\nu)\left(\frac{t}{L}\right)^2\right] \tag{10}$$

$$F_c = 0.7616 - 0.02713 \times \sqrt{\frac{L}{t}} + 0.1083 \cdot \ln\left(\frac{L}{t}\right) \tag{11}$$

Where E is the modulus of elasticity (Pa), L is the sample length (m), t is the sample thickness (m), I is the moment of inertia (kg m^2), ν is the Poisson's ratio, K_s is the measured stiffness (Pa), and F_c is the clamping correction factor.

When using the single cantilever clamp, the equations for stress and strain are:

$$\sigma_x = \frac{3 \cdot P \cdot L}{w \cdot t^2} \tag{12}$$

$$\varepsilon_x = \frac{3 \cdot \delta \cdot t \cdot F_c}{L^2 \left[1 + \frac{12}{5} \cdot (1+\nu) \cdot \left(\frac{t}{L} \right)^2 \right]} \tag{13}$$

Where σ_x is stress (Pa), ε_x is strain, P is the applied force (N), δ is the amplitude of deformation (m), L is the sample length (m), t is the sample thickness (m), w is the sample width (m), F_c is the clamping correction factor, and ν is the Poisson's ratio.

3.2.5 Sampling

For each species, two series of samples were cut from the heartwood part of a green log, one for radial tests and one for tangential tests. Material was sourced from unseasoned boards used for vacuum drying trials of the FWPA project PN08.2047 - *Evaluation of super-heated steam vacuum drying viability and development of a predictive drying model for Australian commercial hardwood species*.

For the radial tests, samples were cut from quartersawn boards, and similarly from backsawn boards for the tangential tests. For each set, samples were cut successively from a board perfectly parallel to the longitudinal direction of the log. This allows similar radial-tangential cross sections to be measured, thus yielding matched samples with very similar properties. Approximately 6 to 10 samples were cut for each species and direction from the centre of green boards. Samples were cut to approximate dimension, 40 mm x 13 mm x 2 mm (Figure 12) using a Struers-Accutom-5™ automatic precision cut-off machine (Plate 7). The machine consists of a rotating saw blade and an electronically adjustable sample feed clamp with a positioning accuracy of 5 µm. Samples were cut under saturated conditions by partially immersing the blade in a water coolant bath. This precaution minimises heating due to friction and subsequent sample drying. Once cut, the samples were immediately wrapped in saturated paper towel, placed in airtight containers and refrigerated. This limited the risk of fungal attack and minimised leaching of wood extractives while samples remain saturated.

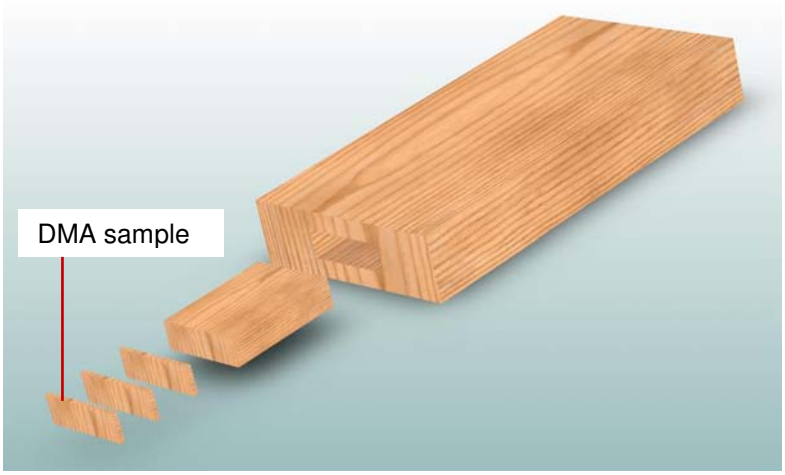

Figure 12. DMA sampling – radial samples shown of approximate dimension, 40 mm x 13 mm x 2 mm.

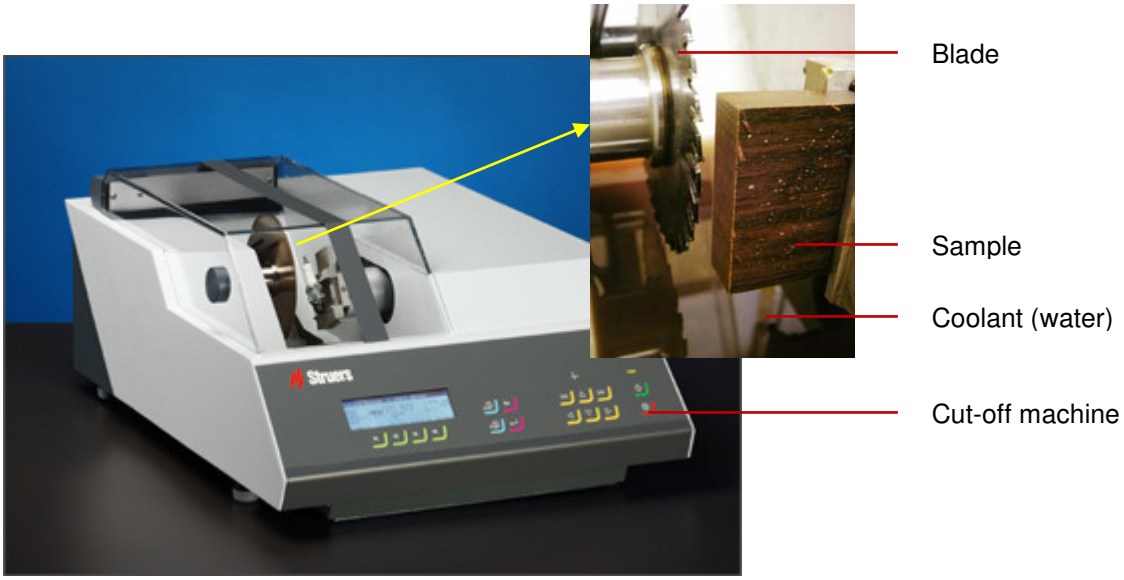

Plate 7. Struers-Accutom-5™ automatic precision cut-off machine.

3.2.6 Experimental procedure

For each species and direction (radial and tangential), three samples were tested. The samples were weighed prior to and immediately after testing to determine moisture content loss. After testing, samples were dried in a laboratory oven at 103 ± 2°C to determine moisture content in accordance with Australian and New Zealand Standard *AS/NZS 1080.1: 1997 Timber – Methods of test – Method 1: Moisture content* (Standards Australia 1997). To minimise moisture loss during testing, samples were wrapped in 3-4 layers of plastic film (Plate 8).

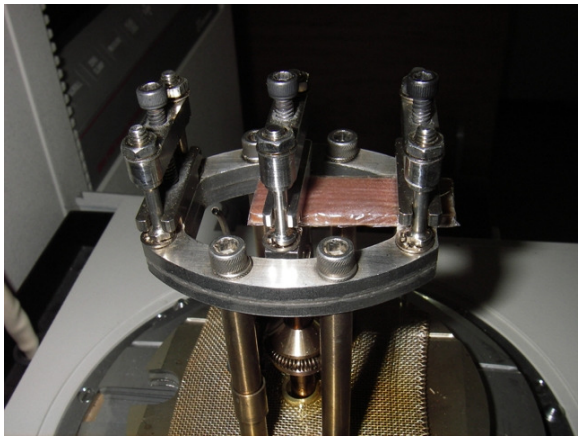

Plate 8. Sample wrapped in plastic film and placed in clamp for DMA testing

Each sample was submitted to multifrequency temperature scans with maximum stress amplitude of 100 µm. The temperature range for each test was 35℃ to 95℃, with a heating rate of 2.0℃/minute and isothermal plateau duration of 1 minute. Measurements were made every 5℃. At each temperature increment, the viscoelastic properties were measured under oscillatory stress at frequencies: 0.1, 1 and 10 Hz. For each frequency the viscoelastic properties E', E" and tanδ were determined.

3.2.6 Determination of glass transition TG

Measurements of tanδ allow the glass transition or softening temperature TG to be determined. When graphed against temperature, the temperature at the peak of the tanδ curve is TG (for an example see Figure 13). As tanδ was measured at 5℃ increments, to accurately determine the temperature of the peak of the tanδ curve, a Gaussian function was fitted using TableCurve 2D™ curve fitting software. The Gaussian function is widely used to determine the peak values of symmetrically shaped curves. The function is of the form:

$$f(x) = a \cdot \exp\left[-\frac{1}{2}\left(\frac{x-b}{c}\right)^2\right] + d \qquad (14)$$

Where a, c and d explain the location and shape (amplitude etc.) of the curve and b is the curve peak (x-axis). Thus, when fitting the Gaussian curve to the tanδ curve, parameter 'b' (equation 14) of the Gaussian function is the glass transition temperature TG.

3.3 Results and discussion

Appendix B contains the full set of viscoelastic results measured and analysed. For each sample (direction and species), the storage modulus (E') and loss factor (tanδ) as a function of temperature are graphically represented. The storage modulus curves begin at the top left corner of the chart and end at the lower right corner. The converse is true for the loss factor curves. Furthermore, each samples dimension, moisture content before and after a test, and glass transition temperature per frequency are provided in Appendix A.

Figure 13 shows a typical example of the storage modulus and loss factor as a function of temperature at different frequencies, shown for *Eucalyptus obliqua* in the tangential direction. These curves uncover the typical characteristics of the viscoelastic behaviour of wood. The storage modulus decreases with increasing temperature and a softening transition appears between 70-100°C. This corresponds to lignin relaxation. The storage modulus curves are perfectly staggered. Indeed, as for all viscoelastic solid materials the modulus of wood increases with frequency due to time dependant molecular relaxation, indicating that the glass transition temperature (peak of tanδ curves) shifts to higher values as the frequency increases (Placet *et al.*, 2007). Furthermore, the glass transition temperature approaches an asymptotic limit with decreasing frequency, indicating that the viscoelastic properties measured at lower frequencies are more representative of static material.

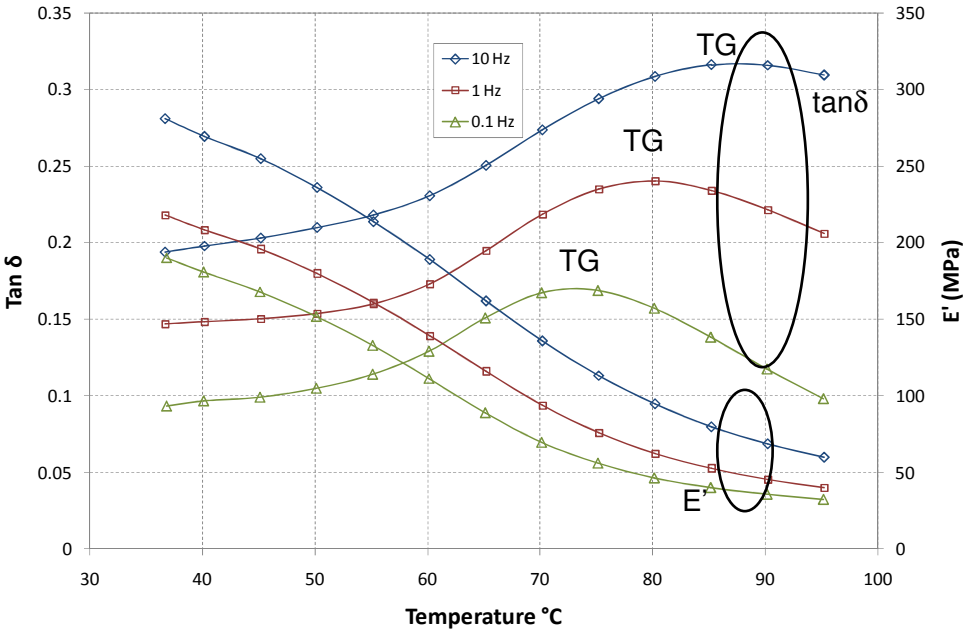

Figure 13. Development of the viscoelastic properties versus temperature of *Eucalyptus obliqua* in the tangential direction.

For some species and directions, at higher frequencies, the glass transition temperature was unable to be determined as it occurs somewhere over 95°C, the maximum temperature tested.

This is most obvious for *Eucalyptus marginata* in the tangential direction where, even for the lowest frequency tested (0.1 Hz), the glass transition temperature could not be determined (Figure 14). To precisely capture the glass transition temperature of this species, two solutions are possible: to perform tests above 95°C or to apply lower frequencies. To perform tests at higher temperatures is problematic with the DMA device used, due to difficulties in maintaining sample moisture contents below fibre saturation points. The option of performing tests at lower frequencies was also unfeasible due to its long duration, and greater potential to induce thermal degradation.

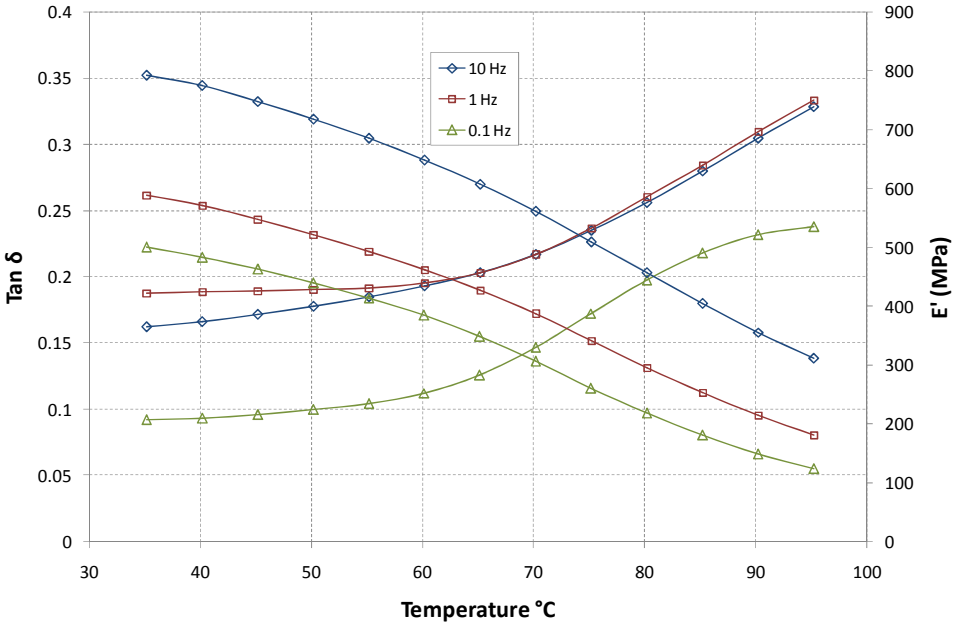

Figure 14. Development of the viscoelastic properties versus temperature of *Eucalyptus marginata* in the tangential direction, showing indeterminable glass transition temperature for every frequency.

As shown in Figure 15, the storage modulus shows a clear difference between the radial and tangential directions, regardless of the frequency, temperature and species. This is consistent with findings reported by Placet et al. (2007). For the species studied, *Corymbia citriodora* was the stiffest, followed in order of reducing stiffness by, *Eucalyptus pilularis, Eucalyptus marginata* and *Eucalyptus obliqua*. These results follow the same trend for static bending evaluation of the modulus of elasticity for these species (Bootle, 2005). The storage modulus was consistently larger in the radial direction than the tangential direction for each species; however the E'_R/E'_T ratio differed between species (Table 2), possibly due to anatomical variations.

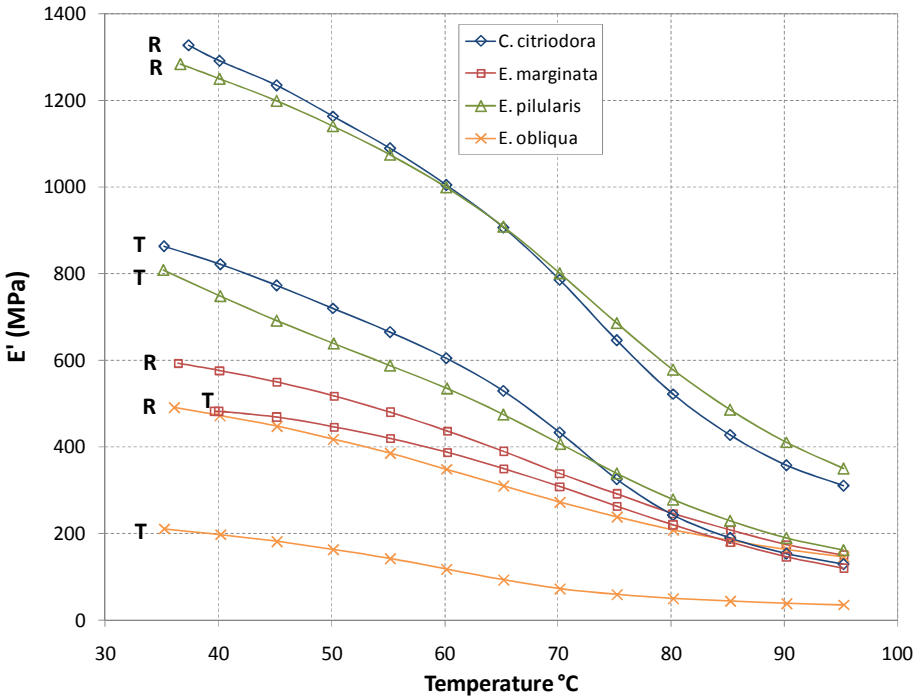

Figure 15. Evolution of the storage modulus versus temperature for each species in the tangential and radial directions (frequency 0.1 Hz).

Table 2. Summary of viscoelastic properties for each species

	C. citriodora		*E. marginata*		*E. pilularis*		*E. obliqua*	
	R	T	R	T	R	T	R	T
Tg (℃)								
0.1 Hz	86.8	86.7		89.7	88.7	87.4	80.4	73.2
1 Hz							90.7	81.1
10 Hz								87.4
E' (MPa) (0.1 Hz)								
Mean	1400	849	687	504	1302	752	485	200
Range	1454-1327	877-805	746-594	531-481	1414-1209	808-680	497-467	211-190
SD	66	38	82	25	104	65	16	10
E'_R/E'_T	1.65		1.36		1.73		2.42	

R, radial; T, tangential; E' measured at 35℃, 0.1 Hz

As shown in table 3, regardless of the wood species and frequency of test, the storage modulus determined from 35℃ to 95℃ decreased less in the radial direction than the tangential direction.

Table 3. Storage modulus values at 35℃ and 95℃ for each species (E' at 0.1 Hz).

	Direction	E' at 0.1 Hz (Mpa)		E'_{35}/E'_{95}	Loss (%)
		35℃	95℃		
C. citriodora	R	1400	318	4.4	77.3
	T	849	128	6.6	84.9
E. marginata	R	687	167	4.1	75.7
	T	504	121	4.2	75.9
E.pilularis	R	1302	349	3.7	73.2
	T	752	157	4.8	79.2
E. obliqua	R	485	147	3.3	69.6
	T	200	34	5.9	83.2

R, radial; T, tangential

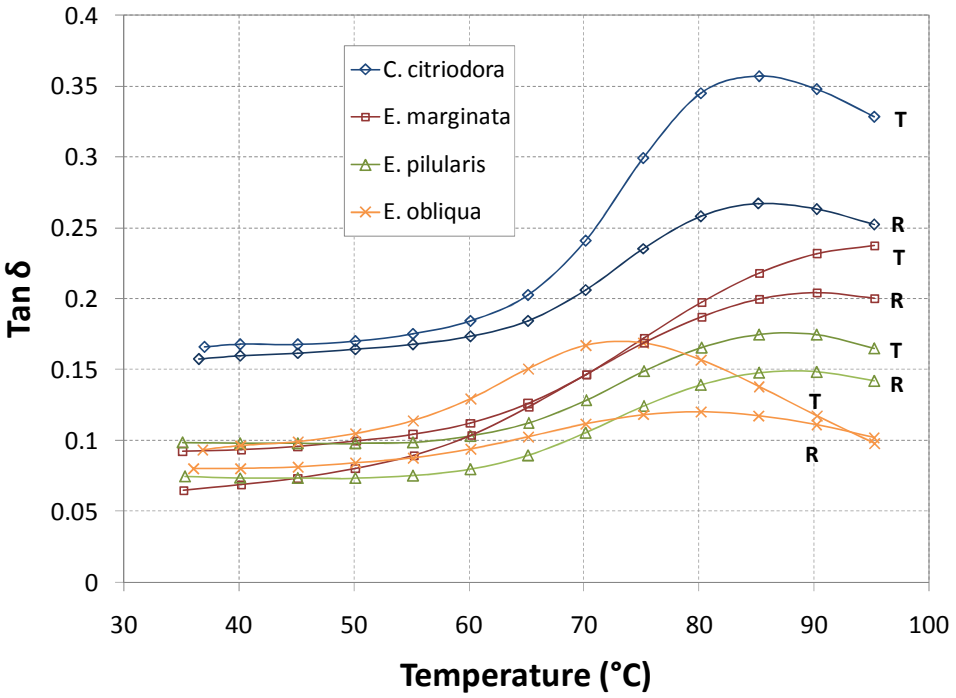

Figure 16. Loss factor versus temperature for each species in radial and tangential directions (frequency 0.1 Hz).

Figure 16 shows the loss factor as a function of temperature (at 0.1 Hz) in the radial and tangential directions. The average glass transition temperatures for each species and test frequency are provided in Table 2. The results show a clear difference in loss factor between the radial and tangential directions, where the tanδ peak was greater in the radial than the tangential direction for all species. Furthermore, the glass transition temperature varied greatly between species with the lowest recorded in the tangential direction for *Eucalyptus obliqua* (73.2℃, at 0.1 Hz) and the highest in the radial direction for *Corymbia citriodora* (> 95℃, all frequencies). Consistent with published data, the glass transition temperature was greater in

the radial direction than the tangential direction, by varying amounts between species. It can be concluded that the internal friction is greater in the radial direction, likely due to enhanced rigidity caused by the presence of radially aligned ray cells (Placet et al., 2007).

The viscoelastic measurements overall revealed many differences in regard to the rheological behaviour of wood, depending on the species and anatomical direction. The greatest influence is caused by the anatomical and molecular features of wood. More precisely, the molecular structure of elemental wood components within the cell wall influences the softening properties. In the temperature range observed, the viscoelastic wood behaviour largely reflects the properties of lignin. In particular the S/G ratio of lignin (explained in section 1.2.3) is thought to heavily influence the glass transition temperature and height of the tanδ curve. To a lesser extent, the microfibril angle of the cell wall layers may also hold influence (Placet et al., 2007).

3.4 Conclusions

- Viscoelastic properties of wood are considerably different in the radial and tangential directions. Consistent with published data, the radial direction shows higher stiffness, internal friction and glass transition temperature than the tangential directions. The loss of stiffness over the measured temperature range was greater in the tangential direction than the radial direction.

- Viscoelastic properties differ between species, largely due to the anatomical and chemical variations between them.

- Consistent with previously published data, due to time dependant molecular relaxation, the storage modulus and glass transition temperature decreases with decreasing frequency, approaching an asymptotic limit. Thus, viscoelastic properties measured at lower frequencies are more representative of static material.

3.5 Further work

At the time of writing this report, the lignin S/G ratio for each species is being investigated to compare with the viscoelastic properties measured. The S/G ratio will be determined using the same samples investigated here.

Chapter 4 – Wood-water relations – shrinkage

4.2 Introduction

The shrinkage of wood during drying is one of the most important properties as it is responsible for deformations during drying (twist, spring, bow and cupping), dimensional variations in situ, and is the driving force for stress. Shrinkage induced drying stress is one of the main reasons for poor quality of dried products.

The work presented in this chapter aims to characterise the wood-water relations of *Corymbia citriodora* (spotted gum), *Eucalyptus pilularis* (blackbutt), *Eucalyptus marginata* (jarrah) and *Eucalyptus obliqua* (messmate), in particular shrinkage. Tests were carried out on small microsamples (1 mm thick) using specialised precision apparatus designed and built to determine the drying behaviour of small micro-samples. By using such small samples, the stress level during testing is not high enough to produce checks and, more importantly the sample can be considered relatively homogeneous particularly in terms of moisture content variation. Furthermore, as far as the author is aware, there are no other methods available to continuously follow the evolution of wood samples as a function of external conditions. The highly accurate results produced by this method are imperative as input parameters for theoretical modelling.

4.3 Materials and methods

4.3.1 Test apparatus

The apparatus used for these tests was designed and built specifically to accurately determine the wood-water relations on micro-samples, by members of the ENGREF team. Plate 9 and Figure 17 present the experimental set-up. The dimensions of micro-samples are measured using a non-contact laser system while continuously measuring the MC of samples.

The system incorporates a highly sensitive electronic microbalance (MC2, Sartorius) with a capacity of 2 g and typical sensitivity of 0.1 µg. Two high speed laser micrometers (Keyance, LS-5000 series) are incorporated to measure changes in the width and height samples without contact. The laser micrometers can measure within a range of 0.2 – 40 mm at a scanning rate of 1200 scans/s, resolution of 0.05 µm and accuracy of 2 µm. The outputs from both devices are fed back to a PC.

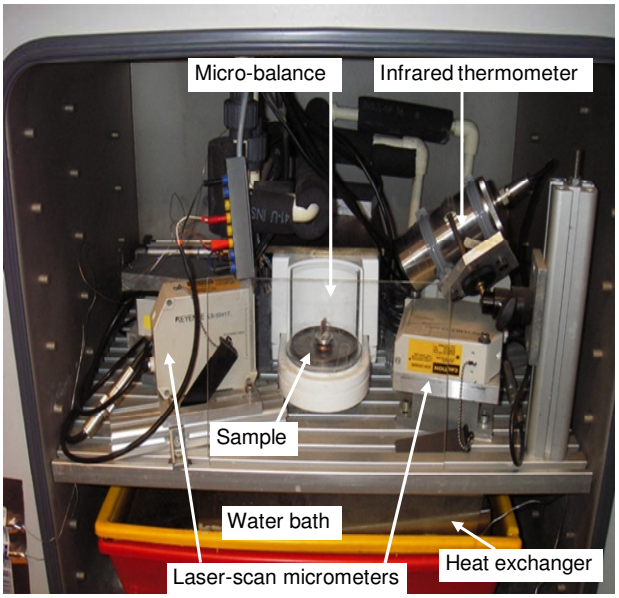

Plate 9. Experimental set-up overview

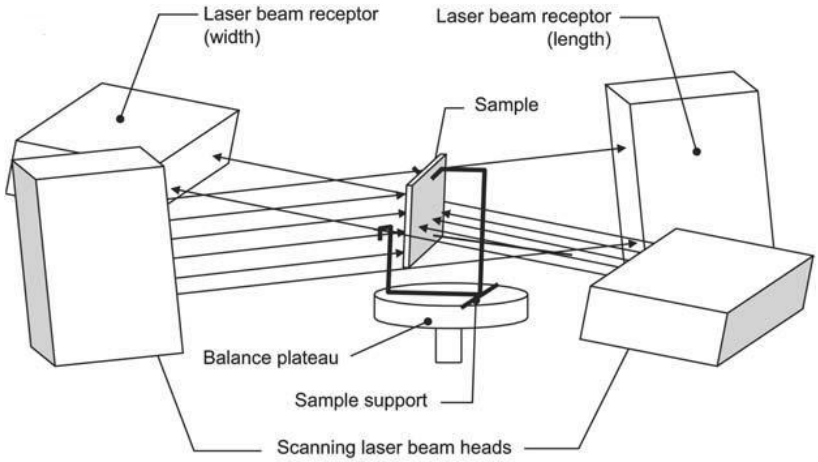

Figure 17. Schematic diagram of scanning laser micrometers and sample positioning. Diagram extracted from Perré (2007).

The surface temperature of samples is measured using an infrared thermometer (pyrometer). It uses a germanium lens with a measurement spot size of 2 mm, and measures to an accuracy of 0.6 % of the measured value (in °C).

The measurement system is placed in a climatic chamber where the temperature is held constant at 30°C by a PID controller. Relative humidity inside the chamber is controlled using a water bath maintained at the desired dew point temperature. A refrigerating circulator is used to maintain the bath temperature. A small fan ensures satisfactory airflow is maintained across the

bath and provides even temperature and humidity conditions throughout the chamber. The dew point and water temperature is measured to an accuracy of 0.1℃ using a dew point analyser.

4.3.2 Sampling

Particular care is required when preparing samples for the apparatus. For each species, a small block of unseasoned material was initially prepared with the approximate dimensions: 13 mm in the tangential (T) direction, 10 mm in the radial (R) direction and 40 mm in the longitudinal direction (L). An additional sample was prepared for *Eucalyptus obliqua,* to investigate longitudinal shrinkage of this collapse prone species, with the following approximate dimensions: 13 mm in the L direction, 10 mm in the T direction and 40 mm in the (R) direction. The block was then sliced in the longitudinal (radial for extra *Eucalyptus obliqua* block) direction using a diamond wire saw (Figure 18) to obtain 1 mm thick samples.

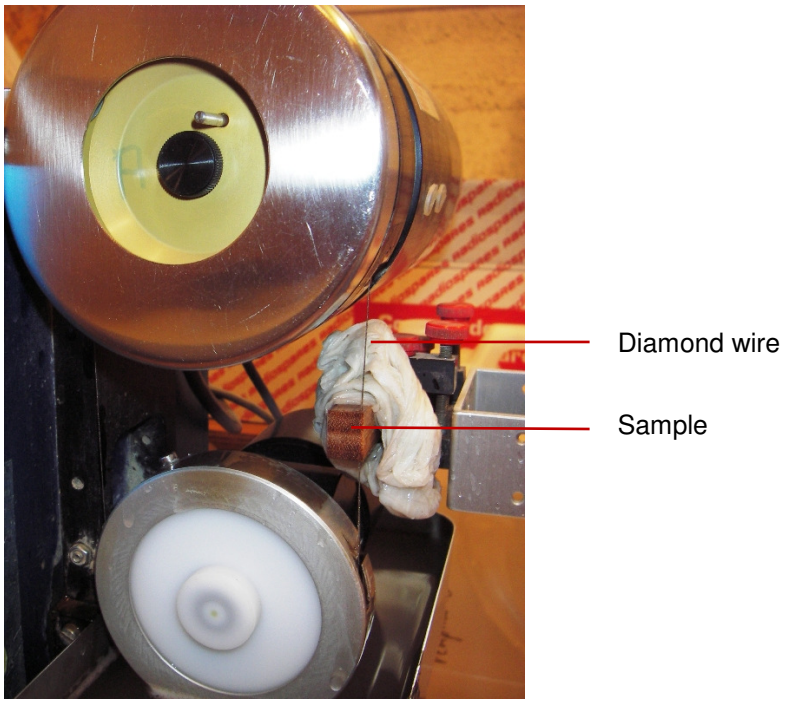

Figure 18. Sample preparation using a diamond wire saw

As the name suggests, the diamond wire saw features a high tensile wire of 0.3 mm diameter in which diamonds, approximately 60 µm wide are impregnated. The wire unwinds and winds between two bobbins. Cutting is performed under a constant load and the wire is submerged in water to minimise heating and drying of the sample. The samples were soaked in water and stored in a refrigerator to minimise fungal attack.

Immediately prior to testing, samples were inserted into a specially designed sample support. The sample support was designed so it does not interfere with the laser beams, shrinkage

measurements are made at the same material locations, and the sample is sufficiently restrained to avoid flexure while maintaining freedom to shrink. Figure 19 shows a sample inserted into the sample support.

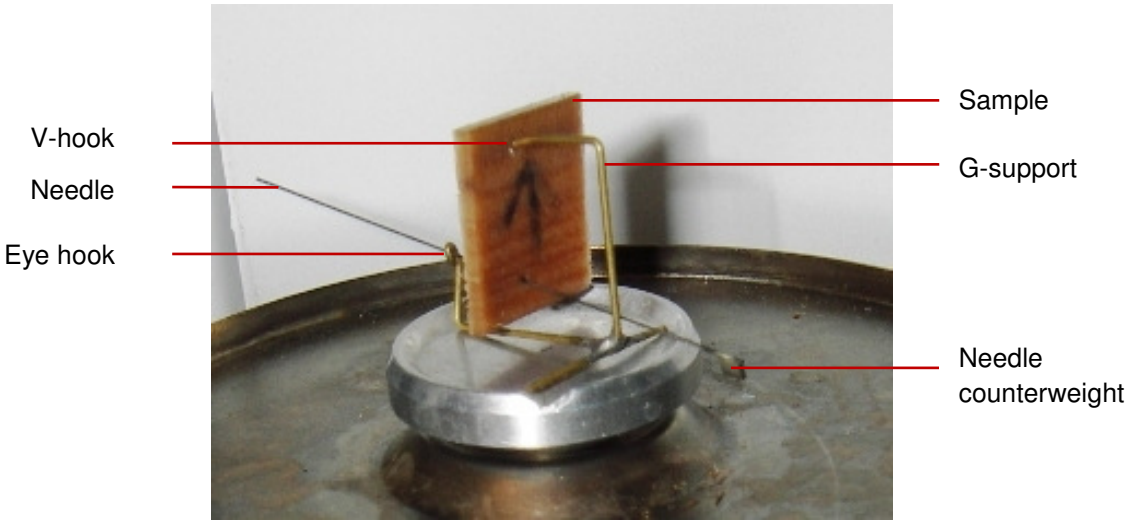

Figure 19. Sample support

The support is made from soldered brass. The sample is hung from a G-shaped support via a 1 mm diameter hole drilled in the upper part. The upper branch of the G-support is curved to create a V shaped hook. The V-shaped hook inhibits sample movement in the direction of the support branch that the V-hook is connected (sample thickness direction). Rotation around the V-hook (sample width direction) is inhibited by using a needle and attached counterweight. The needle is inserted in a second hole (0.8 mm diameter) drilled in the bottom of the sample. One end of the needle is held by an eye-hook at the bottom part of the G-support. The two holes are both offset from the central width of the sample, so that gravity forces the sample to rotate around the V-hook until the needle leans against the G-support. Due to friction, as a result of the needle counterweight, the sample is also blocked from rotating in the direction of the needle. Even though rotational movement of the sample is blocked in all directions it is still free to shrink.

4.3.3 Experimental procedure

Radial and tangential shrinkage was investigated on two samples for each species, except for *Corymbia citriodora*, where three samples were tested due to an unreliable test. Additionally, two tangential and longitudinal shrinkage samples were investigated for *Eucalyptus obliqua*.

Each sample was placed on the support in the centre of the balance, ensuring that the vertical laser passed along the two holes. Drying of the sample before data acquisition was inhibited by regularly adding liquid water to the surfaces using atomised water spray during set-up.

For each test, the water bath was initially set to a temperature of 27°C for 10 hours, then ramped to 9°C over 12 hours, held at these conditions for 3 hours, then returned to 27°C over a

6 hr ramp. The final conditions were held for at least 3 hours. The corresponding relative humidity values were 88% and 30%. The schedule is depicted graphically by Figure 20.

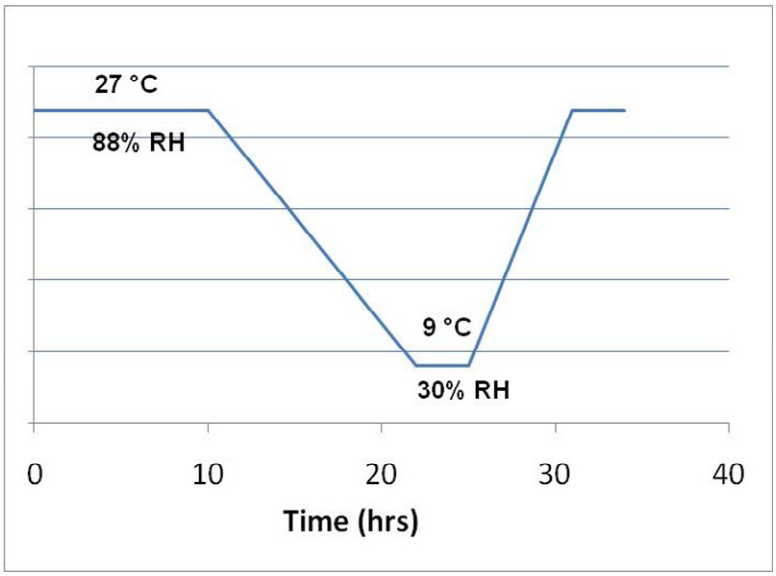

Figure 20. Climatic schedule used for shrinkage tests.

During each test, shrinkage, temperature and sample weight measurements were recorded at regular intervals and stored. At the end of the experiment, the sample was dried at 103 ± 2°C in accordance with *AS/NZS 1080.1* (2001) to determine the current MC of the sample and previous MC evolution during the test.

4.4 Results and discussion

The full series of shrinkage results, represented graphically are provided in Appendix C. For each sample plots of shrinkage, MC and dew point temperature as a function of time and shrinkage as a function of MC are provided.

A typical output of the experimental data is shown in Figure 21 collected for a micro-sample of *Eucalyptus pilularis*. For the first drying cycle, at high relative humidity, very little shrinkage occurs in both the radial and tangential directions, as the samples surface remains above FSP. The sample reaches equilibrium, as shown by the plateau of shrinkage and moisture content, before the shrinkage rate gently increases with decreasing humidity (represented by the dew point temperature). The MC steadily decreases during this period. At the end of the plateau at low relative humidity, the sample picks up moisture and swells. Even though equilibrium is not fully attained, either through desorption or adsorption, a hysteresis effect is apparent, as the MC is less in adsorption than desorption.

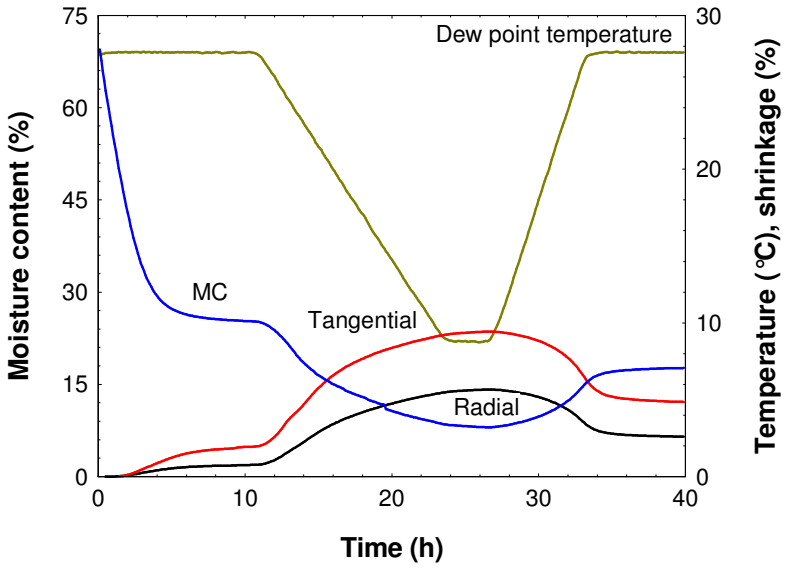

Figure 21. Typical experimental data (MC, tangential and radial shrinkage, and dew point temperature versus time) collected with a *Eucalyptus pilularis* micro-sample.

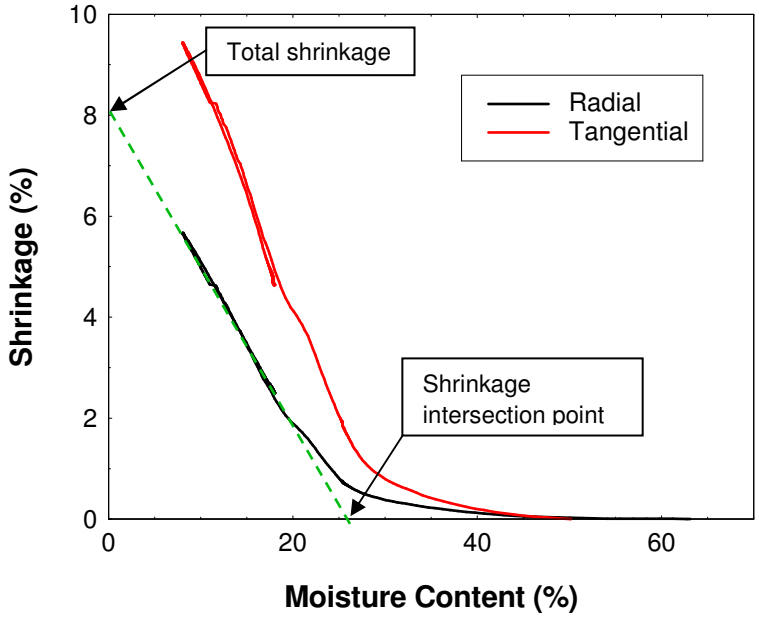

Figure 22. Typical experimental data expressed as shrinkage (radial and tangential) versus MC with a *Eucalyptus pilularis* micro-sample.

The same data can be plotted as a shrinkage versus MC curve as shown in Figure 22. Note that the data defines a very accurate curve during the test period as the adsorption/desorption shrinkage closely follows the same curve (low MC tail of the graph). This lack of hysteresis evident in shrinkage versus MC curves compared to the hysteresis evident in the shrinkage and

MC versus time curves is consistent with published data (Perré, 2007). Observation of the curve distinguishes two different phases: the removal of free water with minimal shrinkage starting above the fibre saturation point, and a noticeable shrinkage phase, denoting the removal of bound water with a linear relationship with MC.

Figure 20 exhibits a typical curve which demonstrates cell collapse during water removal. The species shown is *Eucalyptus obliqua*, a renowned collapse prone species (Bootle, 2005). The radial and tangential shrinkage appears very soon after drying and increase abnormally up to 20-40 % MC. At this point the collapse shrinkage slows down as the sample reaches the bound water domain. Then, in the domain of bound water, normal shrinkage takes place (< 20 % MC). Only this part of the shrinkage is recovered when the sample re-absorbs water. The *Eucalyptus obliqua* collapse results observed are consistent with results observed by Perré (2007) for *Eucalyptus gundal* (*Eucalyptus gunnii x dalrympleana*). It may be possible to avoid collapse shrinkage during shrinkage tests for this species by cutting thinner R-T sections in the longitudinal direction. Clark et al. (2008), observed most eucalypt species have short fibres around 0.6-0.8 mm long. Thus, by reducing the dimension of samples to less than 0.6 mm thickness, the majority of wood fibres will be severed. A cut fibre will not collapse as tension of the cell wall will not be set up if the ends of the fibres are not whole (Redman, 2001).

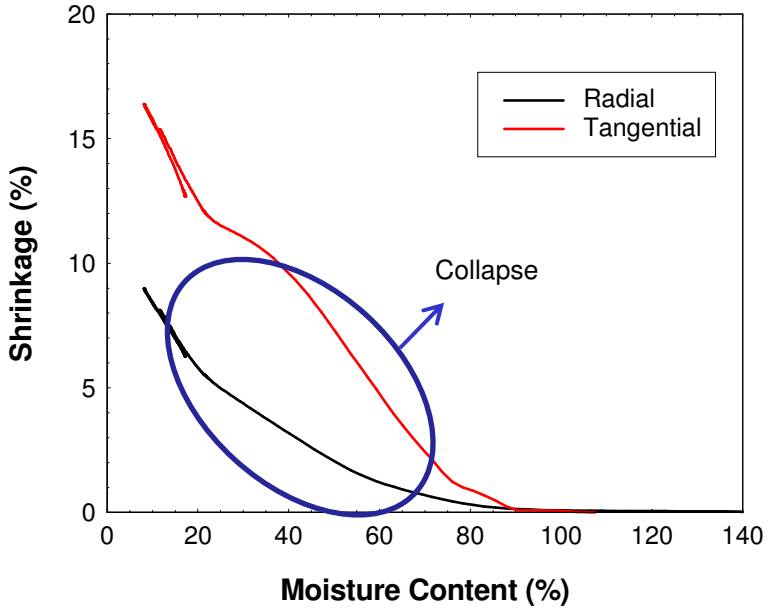

Figure 23. Excessive shrinkage caused by collapse (MC, tangential and radial shrinkage, and dew point temperature versus time) collected with an *Eucalyptus obliqua* micro-sample.

Figure 24, again shows a shrinkage curve for *Eucalyptus obliqua*, this time for the tangential and longitudinal directions. As for the T-R samples, atypical shrinkage due to collapse is present in the tangential direction. The longitudinal direction however, seems unaffected by collapse shrinkage indicating that wood fibres of this species collapse in the radial and

tangential plane of a fibre only. Dimensionally this makes sense, as, similar to an egg, a wood fibre is much stronger when compressed end-to-end (L direction) compared to the sides (R and T directions). Normal shrinkage (unaffected by collapse) in the longitudinal direction is usually very small for strait-grained timber free of reaction wood. As a rough guide, the relationship of the tangential to radial to longitudinal shrinkage is about 100:50:1 (Bootle, 2005).

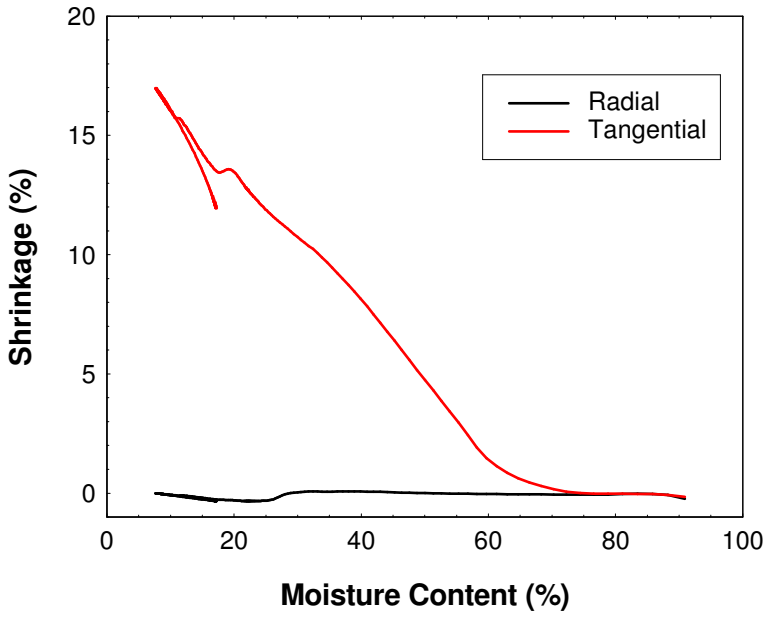

Figure 24. Tangential and longitudinal shrinkage of a *Eucalyptus obliqua* micro-sample

The shrinkage intersection point (also referred to as the fibre saturation point) and total shrinkage can be calculated from the shrinkage versus MC curve by subtending the linear portion of the curve, in the bound water/shrinkage phase, until it intersects the x and y axis (Figure 22). The shrinkage at 12 %, a common published quantification of shrinkage, was calculated from the equation of the subtended line. Table 4 provides the total shrinkage, intersection point and shrinkage at 12 % for each species. Published intersection point and 12% MC shrinkage values are also included, where the published intersection point data is from Budgen (1981) and the shrinkage values at 12 % MC are from Bootle (2005). For the *Eucalyptus obliqua*, samples, the total shrinkage and intersection point could not be calculated due to the presence of atypical collapse shrinkage. Shrinkage measurements were indeterminate for the second *Corymbia citriodora* sample in the tangential direction, due to abnormal sample movement during the test. No published intersection point values were available for *Eucalyptus marginata* or *Eucalyptus obliqua*.

Measured intersection point, total shrinkage and 12% MC shrinkage are consistent within species providing good repeatability. Published intersection point and 12% MC shrinkage values are consistent with measured data. Shrinkage values vary greatly between the tangential and radial directions as expected. Moreover, shrinkage values between species differ due to variations in physical and chemical properties.

Table 4. Shrinkage data measured and published per species (IP: intersection point (%) (Budgen 1981), Total shrinkage and shrinkage at 12 % MC (Bootle 2005))

		Intersection point (%)		IP published (%)		Total shrinkage (%)		Shrinkage at 12 % MC		Published 12 % MC	
Sample #	Species	R	T	R	T	R	T	R	T	R	T
1	*C. citriodora*	23.6	25.9			8.6	8.8	4.4	4.9		
2	*C. citriodora*	24.4	N/A	21.4	24.5	8.4	N/A	4.4	N/A	4.5	6.0
3	*C. citriodora*	24.5	23.0			8.3	8.6	4.5	5.2		
1	*E. marginata*	29.0	34.7			8.2	11.9	4.8	7.8	5.0	7.5
2	*E. marginata*	26.0	34.6			8.4	13.4	4.7	8.9		
1	*E. pilularis*	24.5	31.8	25.1	31.2	8.5	12.6	4.5	7.9	4.0	7.0
2	*E. pilularis*	25.2	30.6			8.4	12.1	4.4	7.3		
1	*E. obliqua*	N/A	N/A			N/A	N/A	N/A	N/A	3.5	6.5
2	*E. obliqua*	N/A	N/A			N/A	N/A	N/A	N/A		

4.5 Conclusions

- Dynamic interactions between relative humidity, moisture content and shrinkage of four Australian hardwood timbers may be usefully monitored on micro-samples using a novel specialised experimental device developed by AgroParisTech – ENGREF, as this generated data consistent with those previously published fro conventional, more laborious methods.

- The novel method generated shrinkage data that varied between species consistent with published data, but were consistent (repeatable) within a species.

- Collapse shrinkage was clearly evident with this method for *Eucalyptus obliqua*, but not with other species, consistent with industrial seasoning experience. To characterise the wood-water relations of this species, free of collapse, thinner sample sections (in the R-T plane) should be used.

4.6 Further work

More shrinkage tests are planned using thinner micro-sample sections of *Eucalyptus obliqua* (approximately 0.5 mm) to measure the wood-water relations of this species free of collapse shrinkage. This is critical to provide accurate input values for the wood drying model under development.

References

Australian and New Zealand Standard *AS/NZS 1080.1:1997 Timber - Methods of test: - Method 1: Moisture content.*

Australian and New Zealand Standard *AS/NZS 1080.3:2000 Timber – Methods of test – Method 3: Density.*

Aguiar O., Perré P. (2000). Wood accelerating drying process based on its rheological properties, CE: B27K5/00; F26B21/06.

Badel E., Perré P. (2007). The shrinkage of oak predicted from its anatomical pattern: model validation, Trees, structure and functions, 21:111–120.

Baettig, R., Rémond, R. and Perré, P. (2006). Measuring moisture content profiles in boards during drying: a polychromatic x-ray system interfaced with a vacuum/pressure laboratory kiln. Wood Science and Technology 40:261-274.

Budgen, B. (1981). Shrinkage and density of some Australian and South-east Asian timbers. CSIRO technical paper No. 38, CSIRO, Australia.

Bootle, K.R. (2005). *Wood in Australia, types, properties and uses*. Second edition. McGraw-Hill. Sydney.

Butterfield, B.G. and Meylan, B.A. (1980). *Three dimensional structure of wood*. Chapman and Hall, USA.

Clarke, C.R.E., Palmer, B. and Gounden, D. (2008). Understanding and adding value to *Eucalyptus* fibre. Southern Forests: a Journal of Forest Science, 70(2): 169-174(6).

Cronshaw, J. 1960. The fine structure of the pits of *Eucalyptus regnans* (F. Muell) and their relation to the movement of liquids into the wood. *Aust. J. Bot.*, Vol8, No.1.

Ehrenstein, G.W. and Montague, F. (2000). Matériaux polymères. Structures, propriétés et applications, 351 pp, edited by H.S. publications, Paris.

Hamdan, S., Dwianto, W., Morooka, T., and Norimoto, M. (2000). Softening characteristics of wet wood under quasi static loading. *Holzforschung* 54(5): 557-560.

Irvine, G.M. (1984). The glass transitions of lignin and hemicellulose and their measurement by differential thermal analysis. *Tappi Journal* 67(5): 118-121.

Lenth, C. A., Kamke, F. A. (2001). Moisture dependent softening behavior of wood. *Wood and Fibre Science* 33(3): 492-507.

Nolan, G. Innes, T.C., Redman, A.L. and McGavin, R. (2003). Australian hardwood drying best practice manual. Project no: PN01.1307. University of Tasmania and Department of Primary Industries and Fisheries report prepared for Forest and Wood Products Australia.

Perré, P. and Turner, I. (1999a). TransPore: A generic heat and mass transfer computational model for understanding and visualising the drying of porous media. Drying Technology Journal, *17*(7), 1273–1289.

Perré, P. and Turner, I. (1999b). A 3D version of TransPore: A comprehensive heat and mass transfer computational model for simulating the drying of porous media. Int. J. Heat Mass Transfer, *42*(24), 4501–4521.

Perré, P. (2005). *MeshPore*. A software able to apply image-based meshing techniques to anisotropic and heterogeneous porous media, Drying Technology 23: 1993-2006.

Perré, P., and Rémond R. (2006). A dual scale computational model of kiln wood drying including single board and stack level simulation. Drying Technology 24: 1069-1074.

Perré, P. (2007). Experimental device for the accurate determination of wood-water relations on micro-samples. Holzforchung, 61: 419-429.

Placet, V. (2006). Conception et exploitation d'un dispositive expérimental innovant pour la caractérisation du comportement viscoélastique et de la dégradaton thermique du bois dans des conditions sévères. PhD thesis. Docteur de l'Université Henri Poincaré, Nancy-1.

Placet, V., Passard, J., and Perré, P. (2007). Viscoelastic properties of green wood across the grain measured by harmonic tests in the range of 0-95°C: Hardwood vs. softwood and normal wood vs. reaction wood. Holzforschung. 61: 548-567.

Placet, V., Passard, J., and Perré, P. (2008). WAVE^{*T}, a custom device able to measure viscoelastic properties of wood under water saturated conditions (*WAVE^{T} : Environment Vibration Analyser for Wood). Maderas. Ciencia y technología. 10(1): 45-60.

Redman, A.L. (2006). Superheated steam vacuum drying. Paper presented at the DryTech 2006 Tools and Technologies to Improve Timber Drying conference, 27-28 November, 2006, Melbourne, Australia.

Redman, A.L. and McGavin, R. (2008). Evaluation of wood characteristics of tropical post-mid rotation plantation *Eucalyptus cloeziana* and *E. pellita*: Part (b) Accelerated seasoning of sawn timber. Project no: PN07.3022. Department of Primary Industries and Fisheries report prepared for Forest and Wood Products Australia.

Redman, A.L. (2001). Improving quality of of seasoned Tasmanian eucalypt species. Master thesis for the Faculty of Engineering, University of Tasmania.

Ressel, J.B. (2008). Wood anatomy – an introduction. Book chapter from: *Fundamentals of Wood Drying*. Ed. Perré, P. A.R.BO.LOR ENGREF, France.

Savard, M., Lavoie, Lavoie, V. and Trembala, C. (2004). Technical and Economical Assessment of Superheated Steam Vacuum Drying of Northern Red Oak. P. 1-10 in N.A.G.R.E.F. COST E15 Conference. Forintel Canada Corp., Athens, Greece.

Siau, C. (1984). *Transport processes in wood.* Springer-Verlag, Germany.

Skaar, J.F. (1988). *Wood-water relations*. Springer-Verlag, USA.

Vermaas, H.F. (1995). Drying eucalypts for quality: Material characteristics, pre-drying treatments, drying methods, schedules and optimisation of drying quality. South African Forestry Journal, 174, 41-49.

Appendix A – ESEM Images

Corymbia citriodora (spotted gum)

200 x magnification

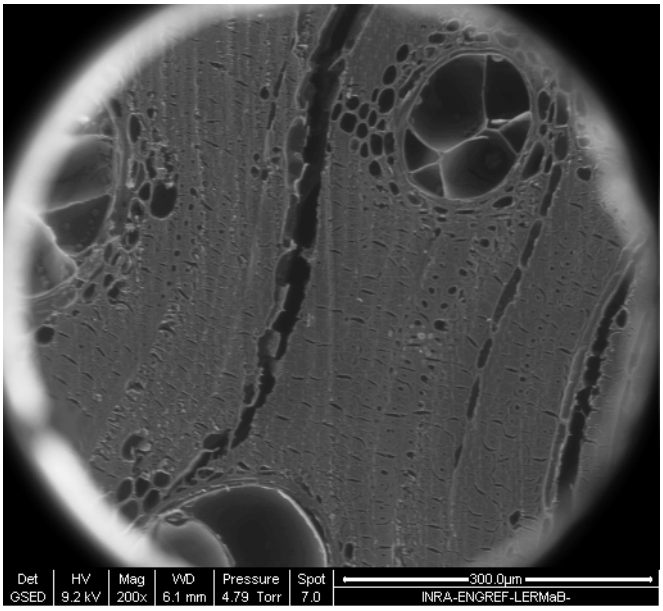

400 x magnification

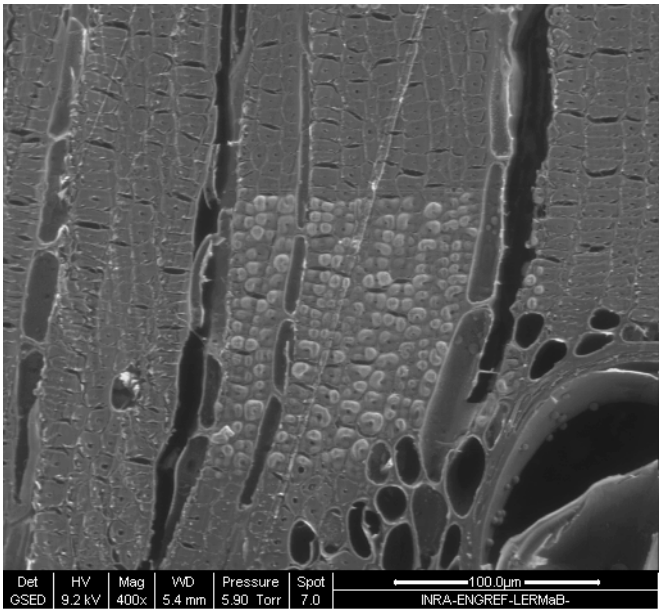

800 x magnification

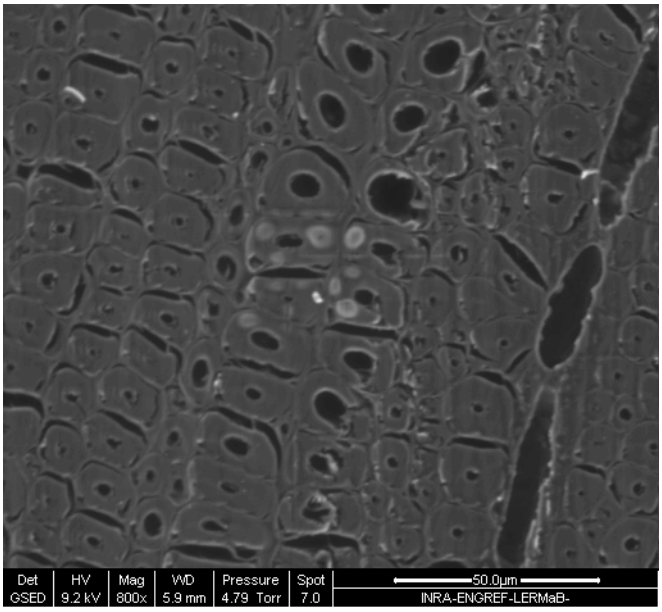

Eucalyptus marginata (jarrah)

200 x magnification

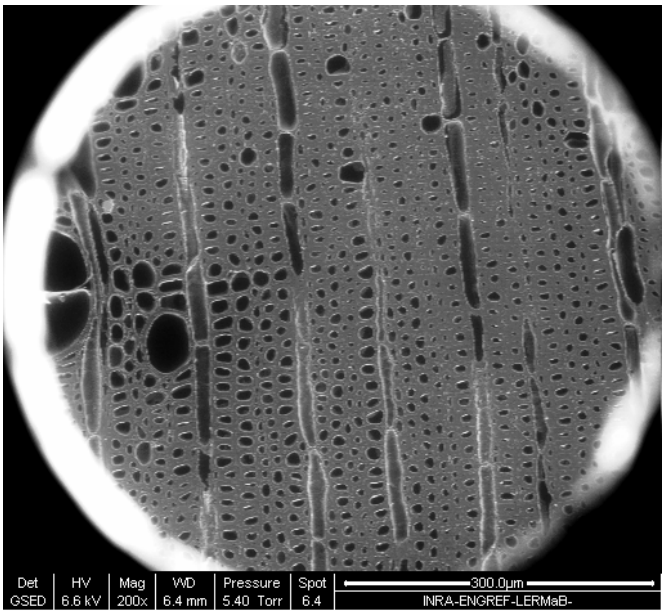

400 x magnification

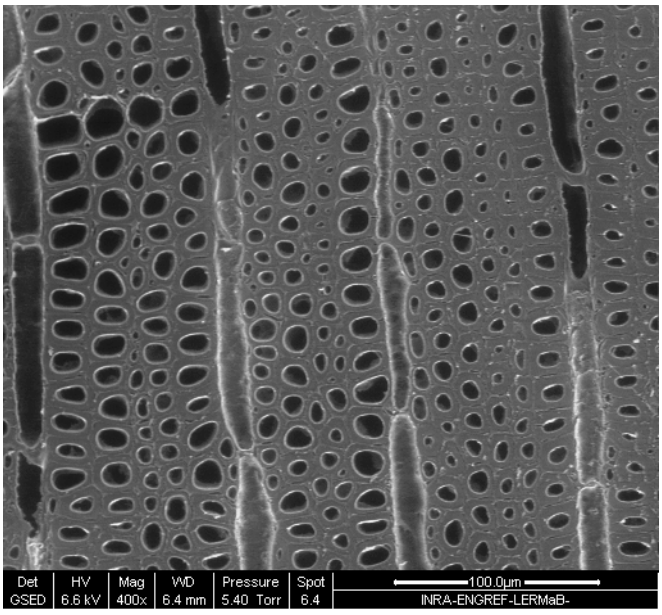

800 x magnification

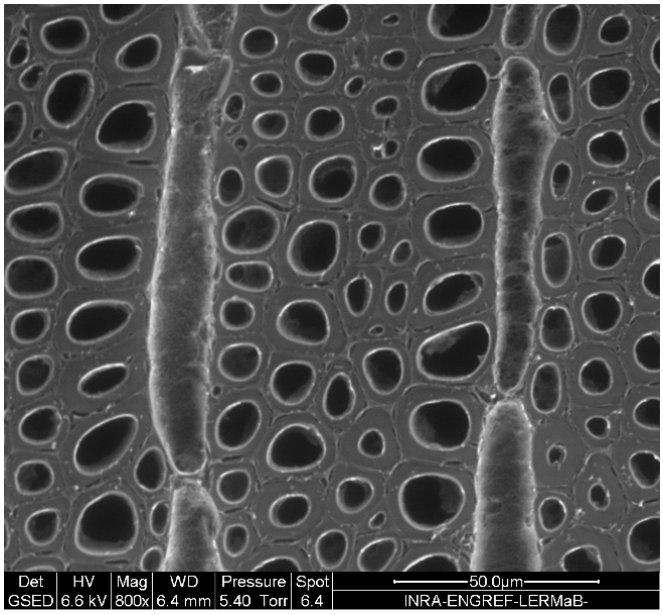

Eucalyptus pilularis (blackbutt)

200 x magnification

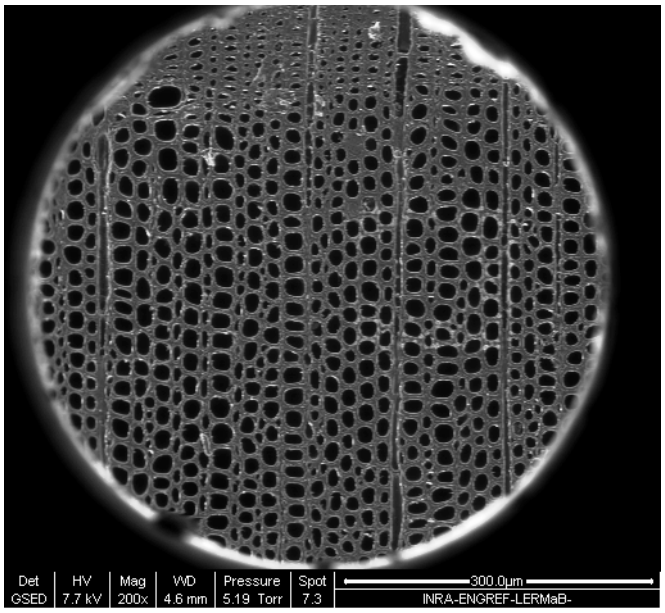

400 x magnification

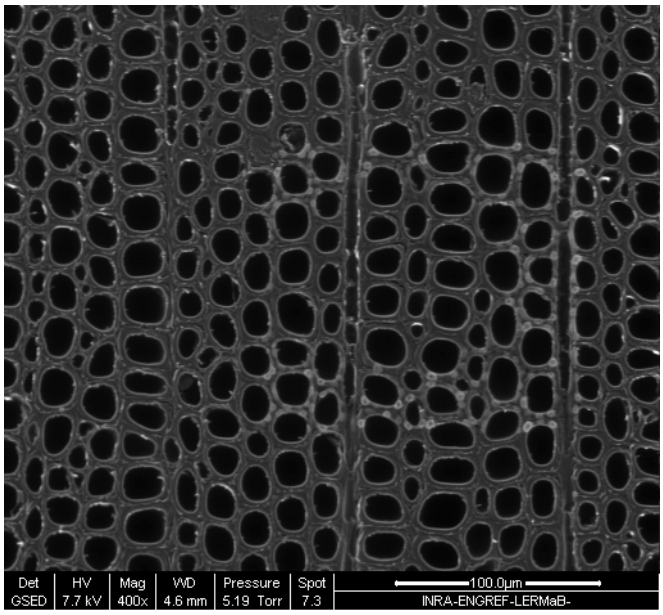

800 x magnification

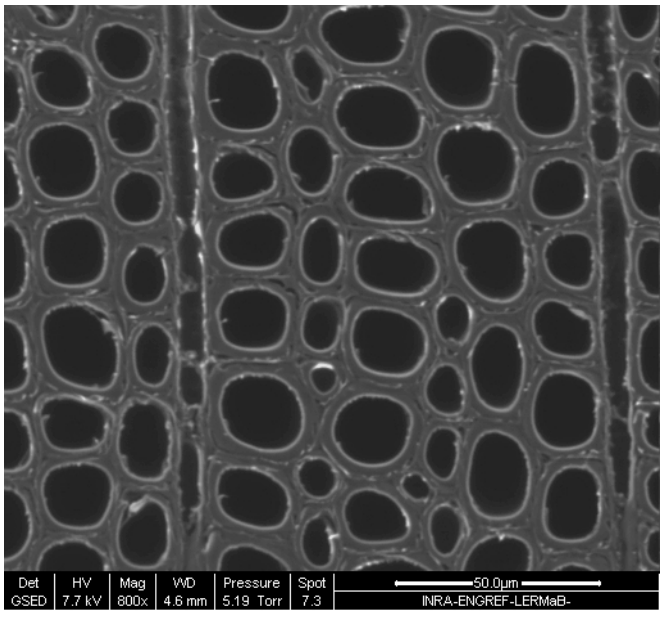

Eucalyptus obliqua (messmate)

200 x magnification

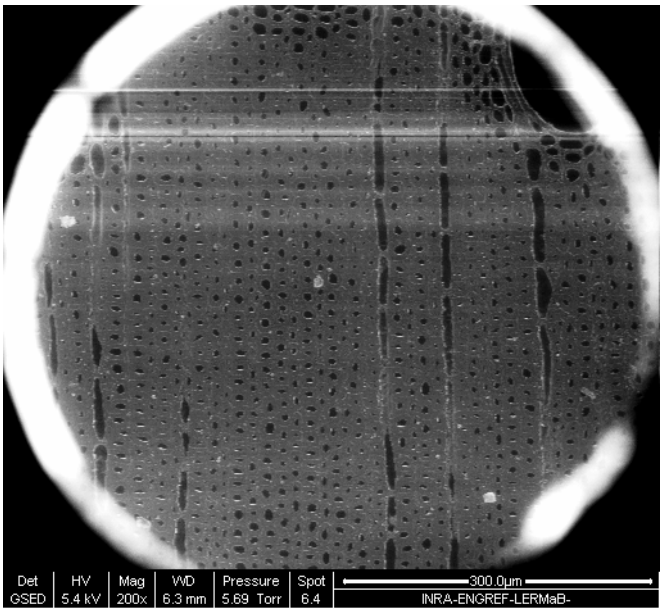

400 x magnification

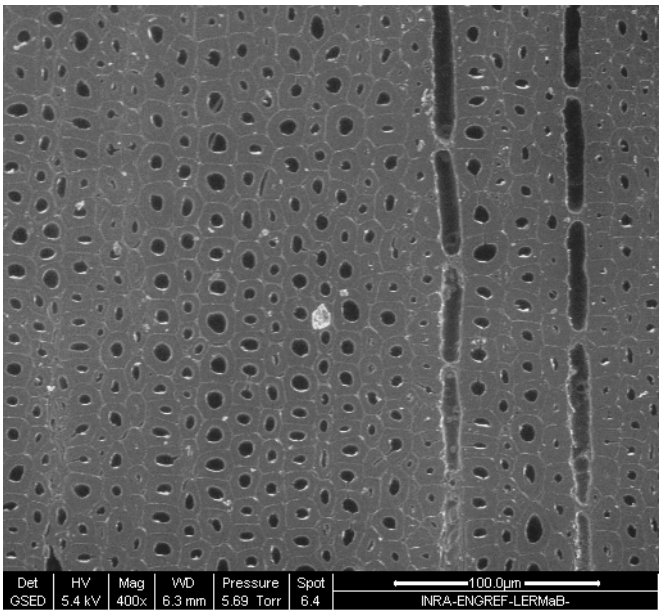

800 x magnification

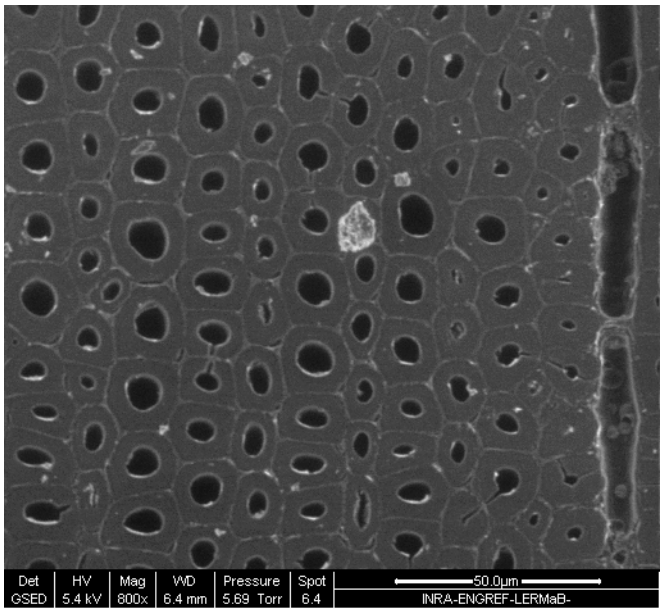

Appendix B – DMA Results

Corymbia citriodora (spotted gum) – DMA tangential

Sample 1

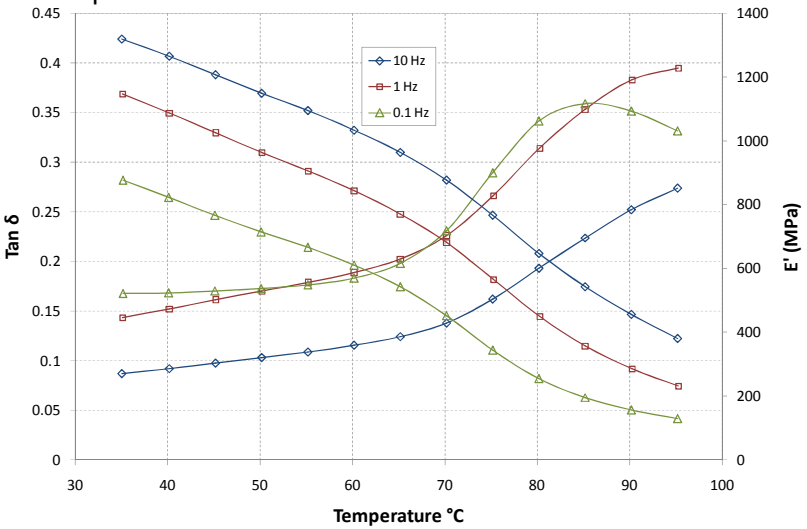

Sample 2

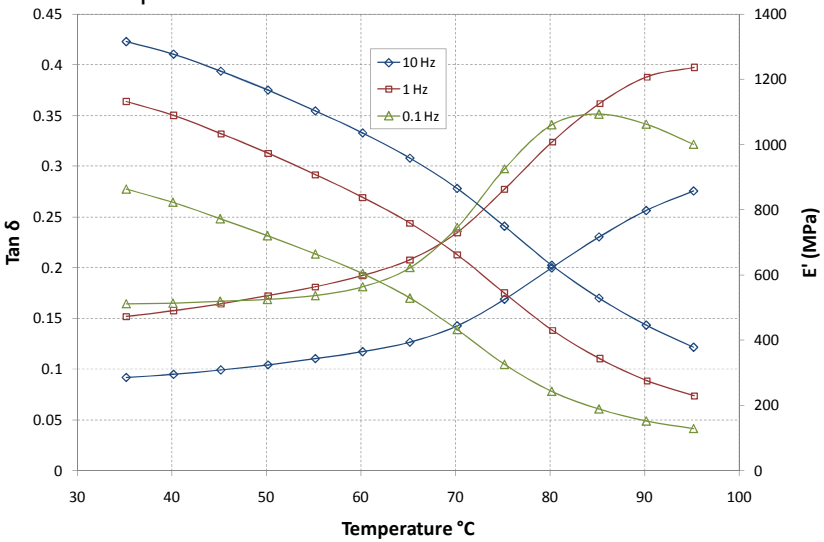

Sample3

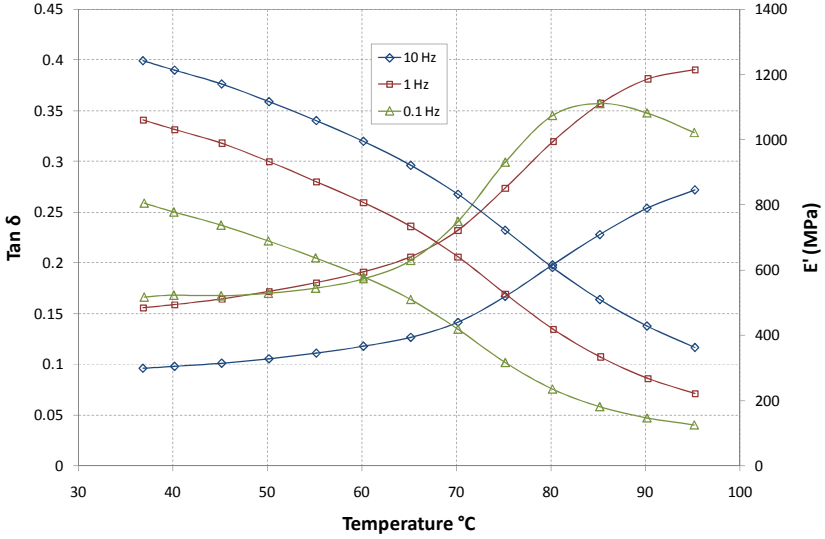

C. citriodora Tangential Sample	Moistrue content (%)		Dimension (mm)					
	Before DMA	After DMA	Before DMA			After DMA		
			Length	Width	Thickness	Length	Width	Thickness
1	62.0	48.1	39.83	12.30	2.12	39.87	12.21	2.12
2	61.5	48.2	39.82	12.34	2.08	39.85	12.28	2.13
3	61.0	52.9	39.81	12.33	2.08	39.90	12.34	2.08

C. citriodora Tangential Sample	Tg (°C) 0.1 Hz	
	Gaussian	r^2
1	87.1	0.996
2	86.4	0.996
3	86.6	0.996
Average	**86.7**	**0.996**

Corymbia citriodora (spotted gum) – DMA Radial

Sample 1

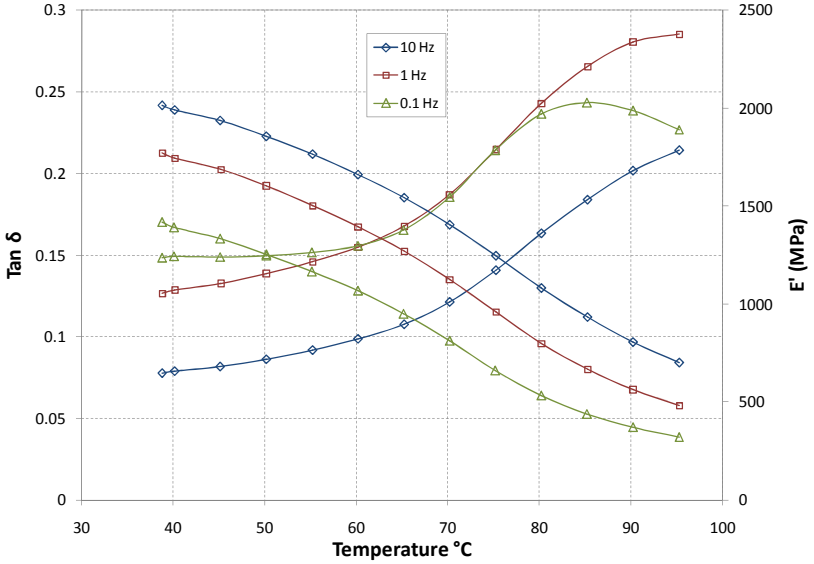

Sample 2

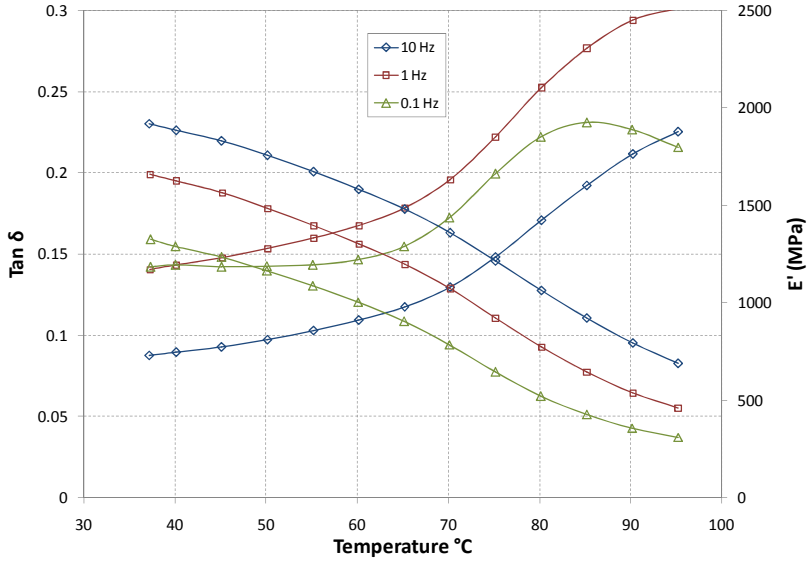

Sample 3

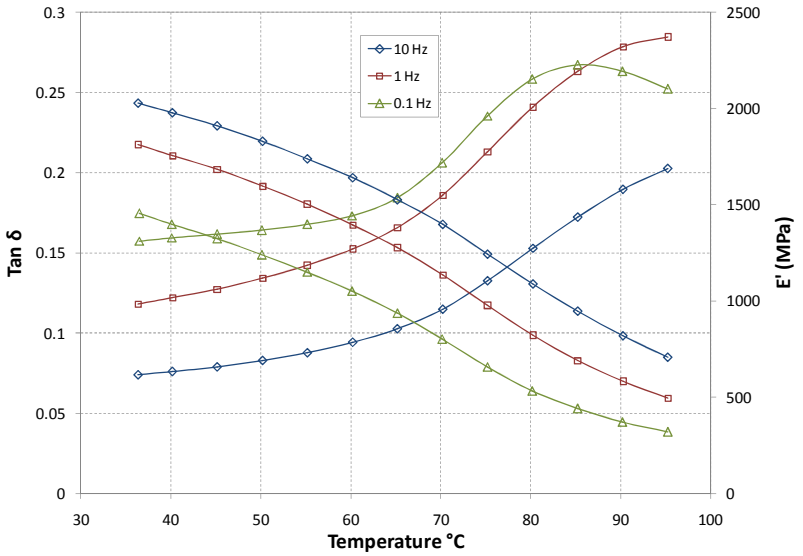

C. citriodora Radial Sample	Moistrue content (%)		Dimension (mm)					
	Before DMA	After DMA	Before DMA			After DMA		
			Length	Width	Thickness	Length	Width	Thickness
1	48.9	37.0	35.69	12.53	2.03	35.59	12.64	2.03
2	51.5	37.3	35.50	12.81	2.07	35.31	12.83	2.08
3	49.9	41.0	35.63	12.72	2.07	35.05	12.72	2.07

C. citriodora Radial Sample	Tg (°C) 0.1 Hz	
	Gaussian	r^2
1	86.5	0.997
2	86.9	0.997
3	87.0	0.997
Average	**86.8**	**0.997**

Eucalyptus marginata (jarrah) – DMA tangential

Sample 1

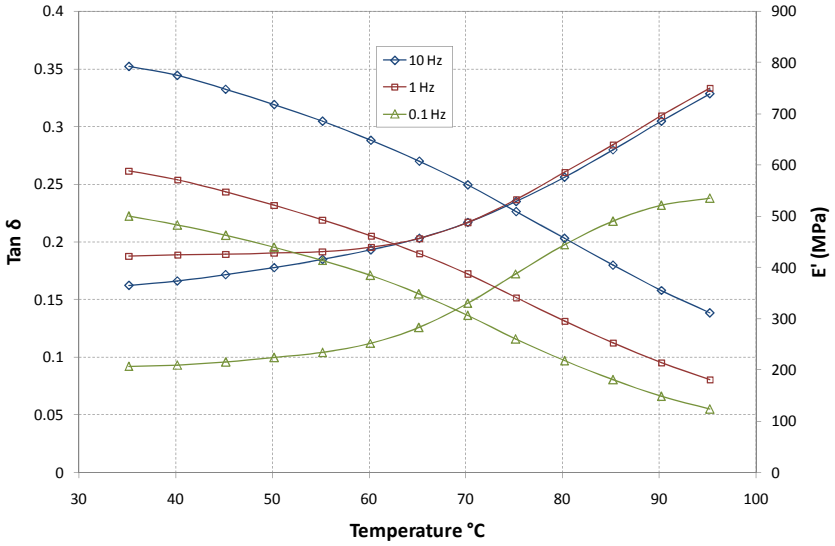

Sample 2

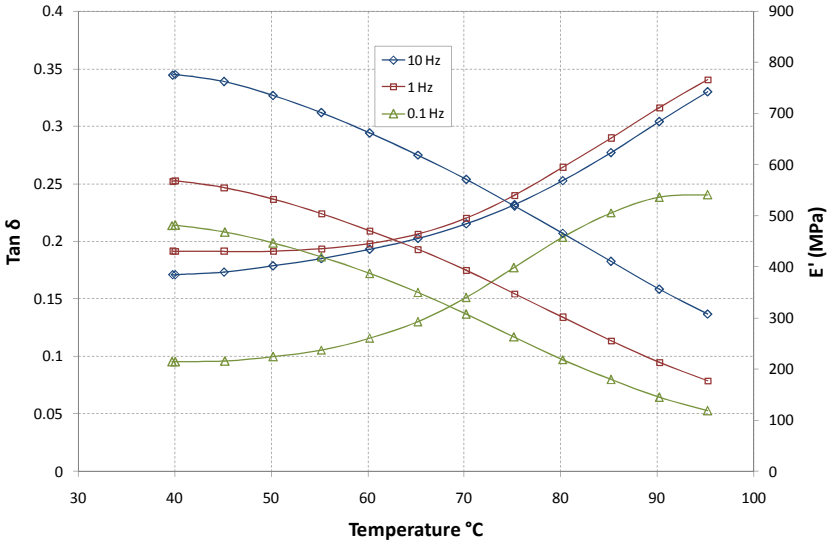

Sample 3

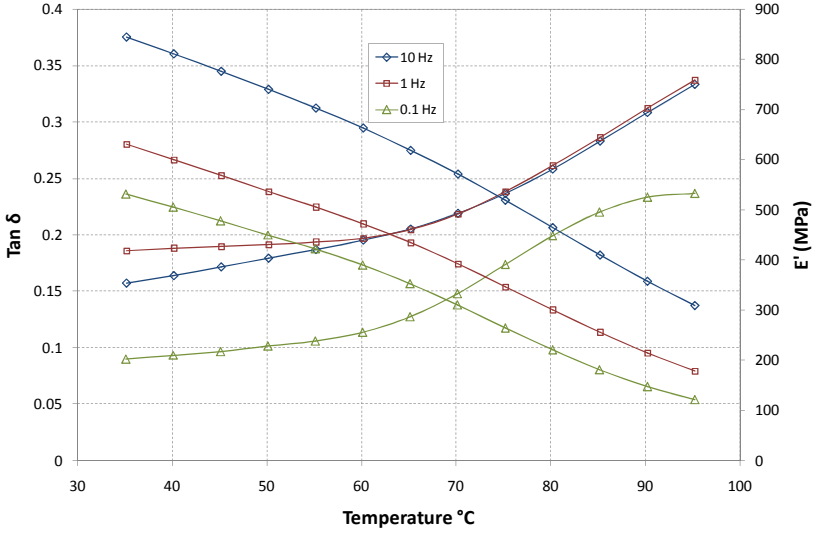

[redacted]

[redacted]

Eucalyptus marginata (jarrah) – DMA radial

Sample 1

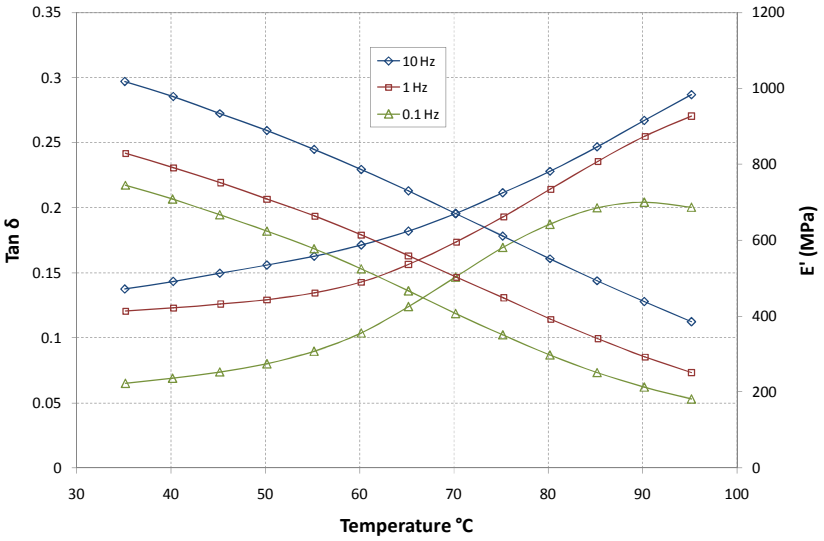

Sample 2

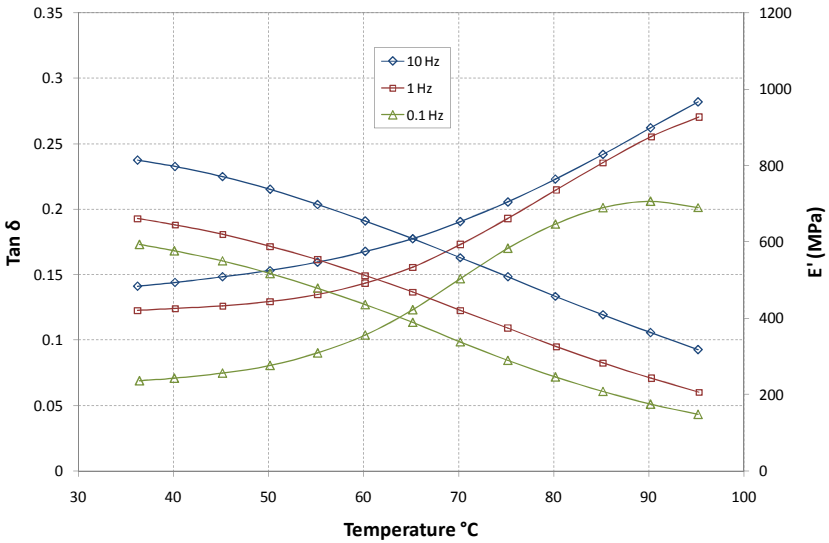

Sample 3

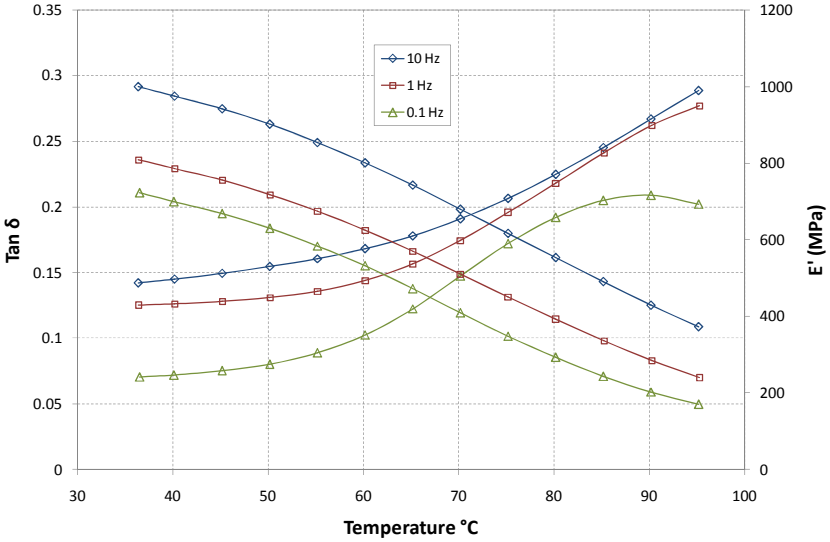

[redacted]

E. marginata Radial Sample	Tg (°C) 0.1 Hz	
	Gaussian	r^2
1	90.0	0.999
2	89.8	0.999
3	89.2	0.999
Average	**89.7**	**0.999**

Eucalyptus pilularis (blackbutt) – DMA tangential

Sample 1

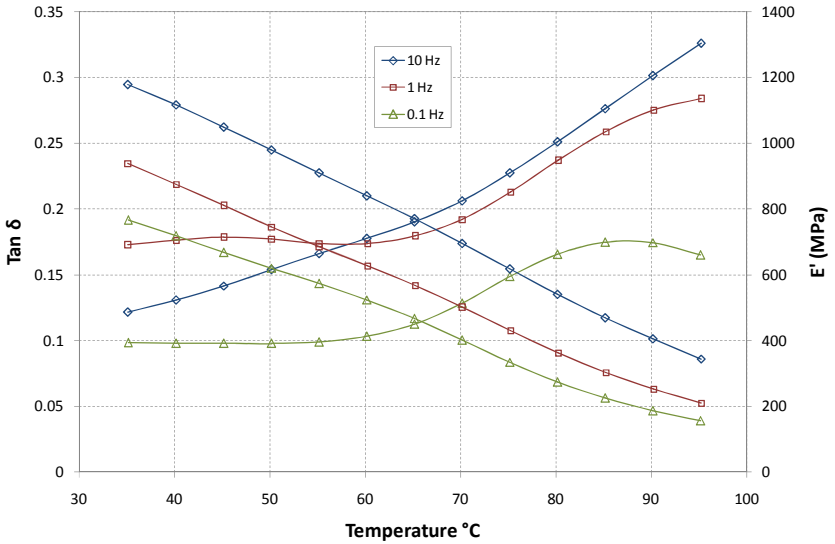

Sample 2

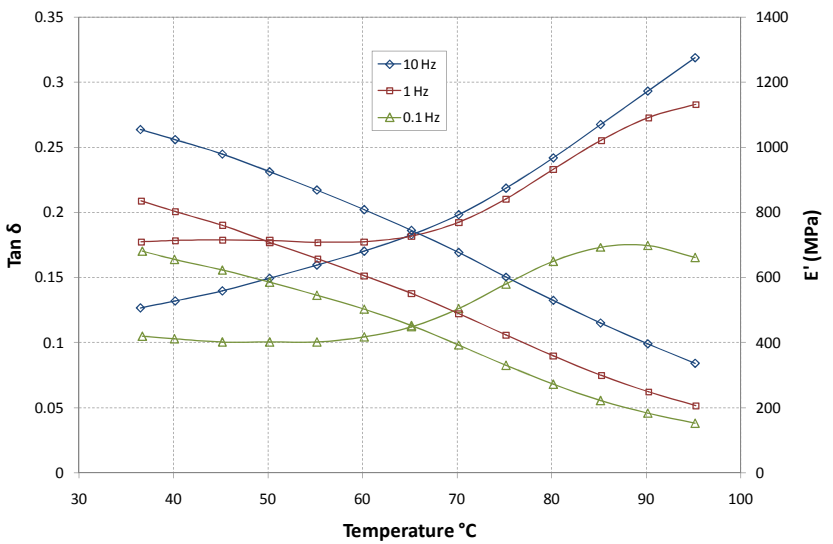

Sample 3

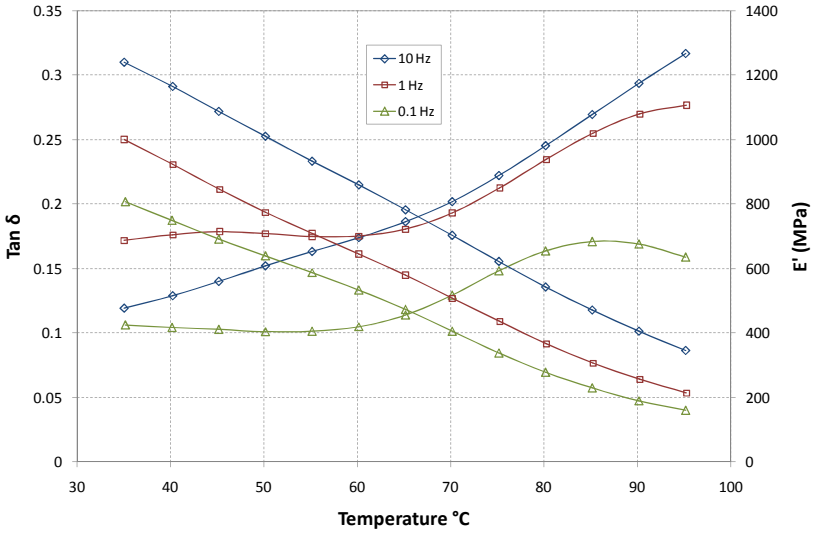

[redacted]

[redacted]

Eucalyptus pilularis (blackbutt) – DMA radial

Sample 1

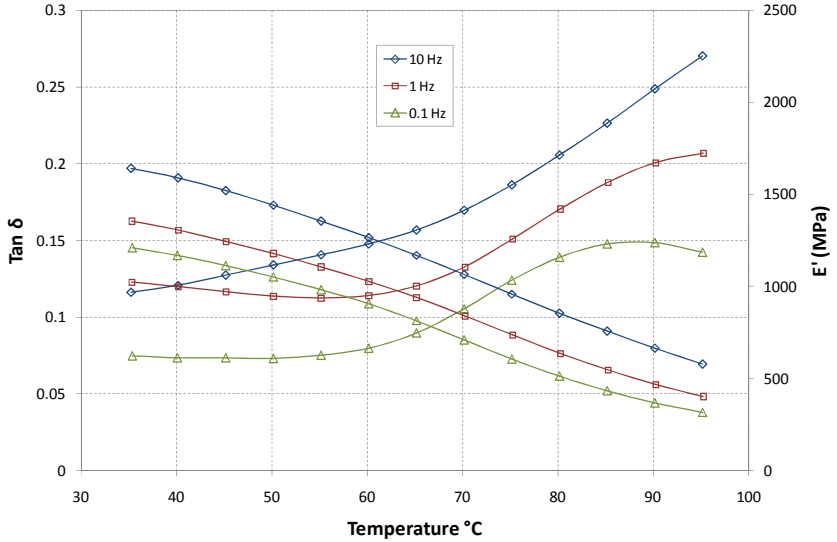

Sample 2

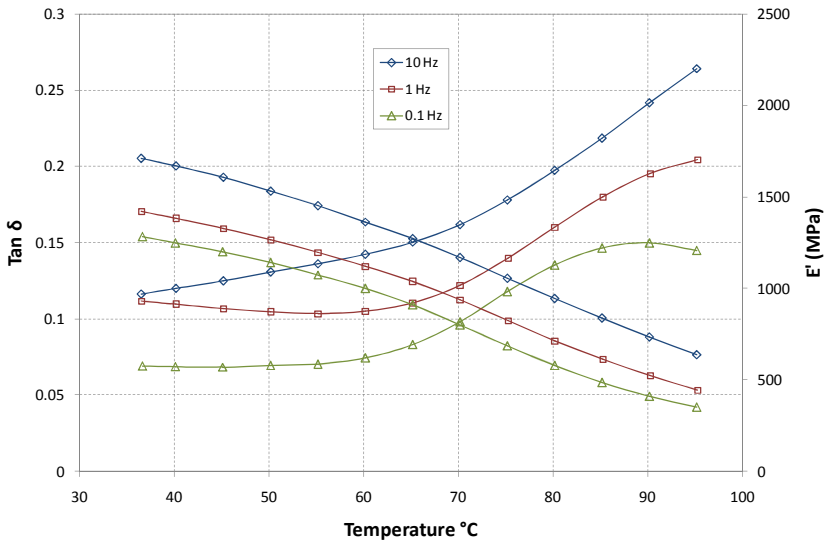

Sample 3

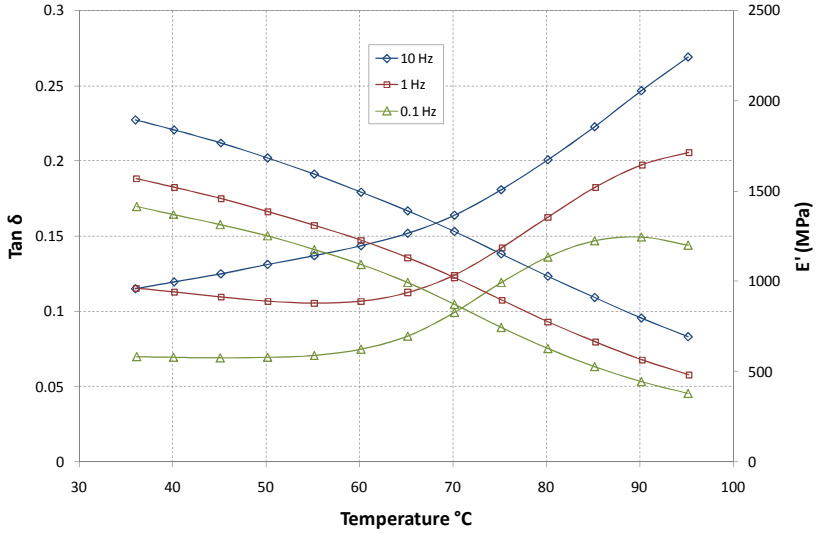

[redacted]

[redacted]

Eucalyptus obliqua (messmate) – DMA tangential

Sample 1

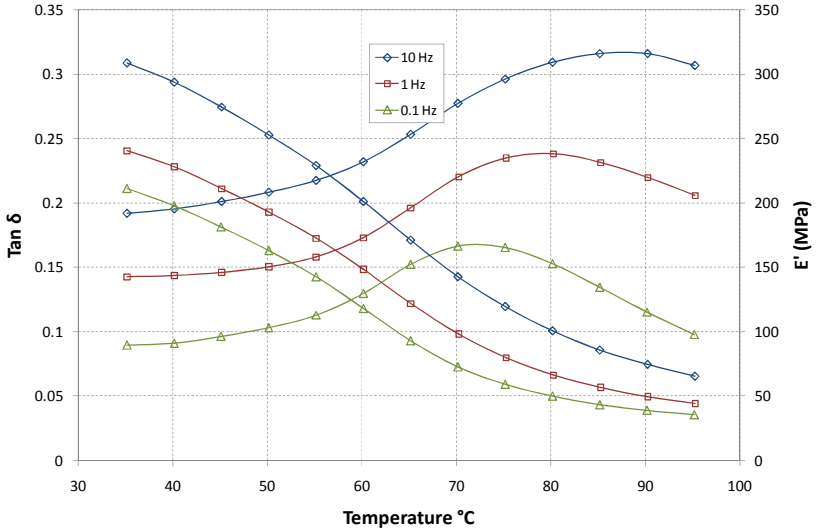

Sample 2

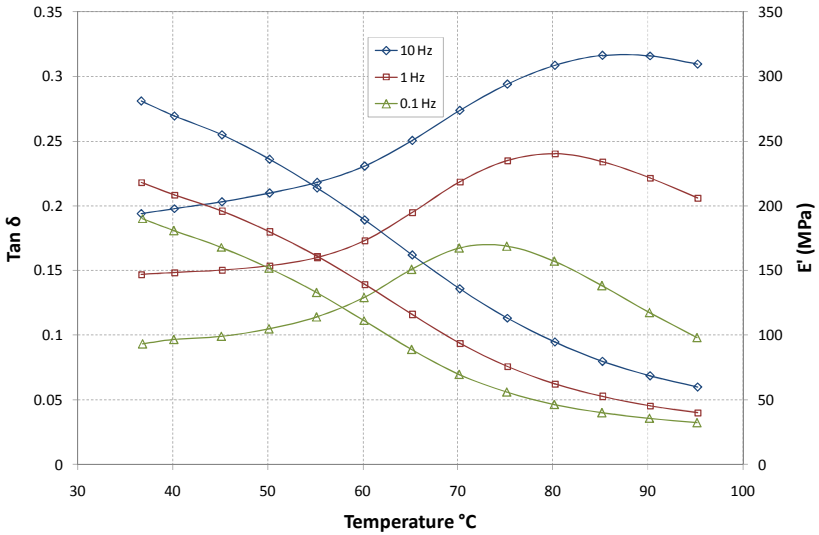

Sample 3

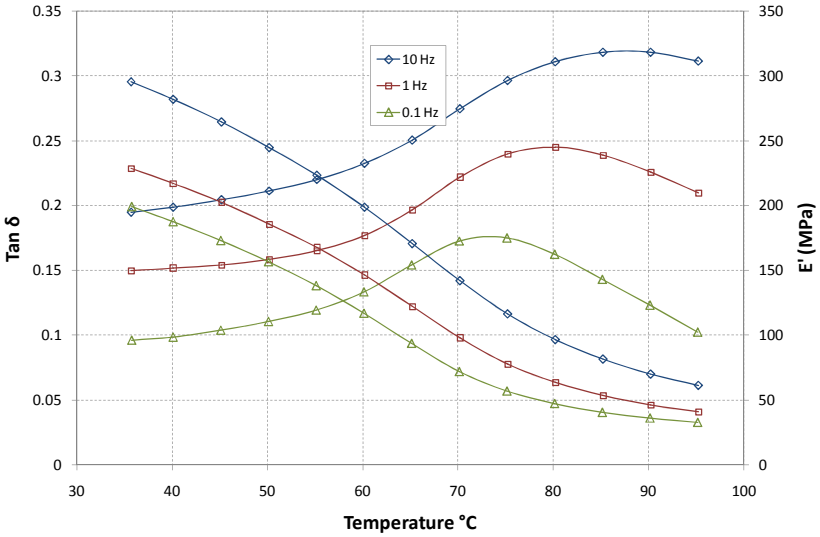

[redacted]

[redacted]

Eucalyptus obliqua (messmate) – DMA radial

Sample 1

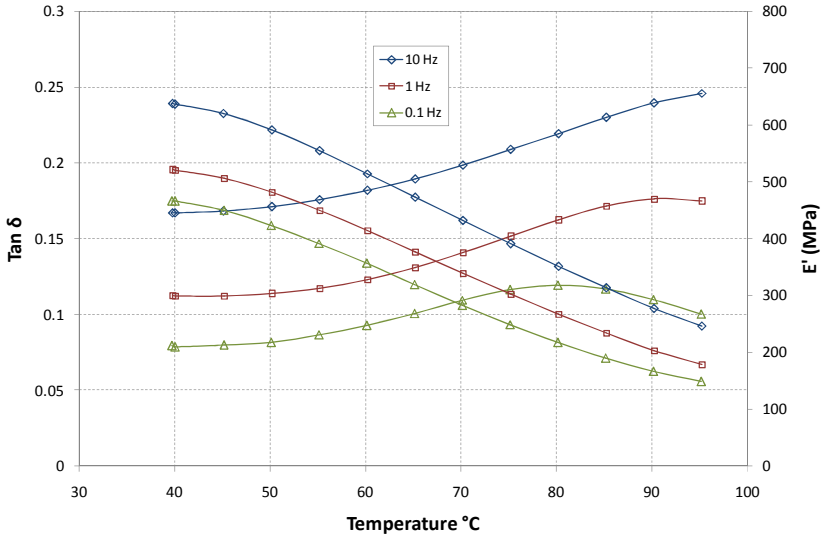

Sample 2

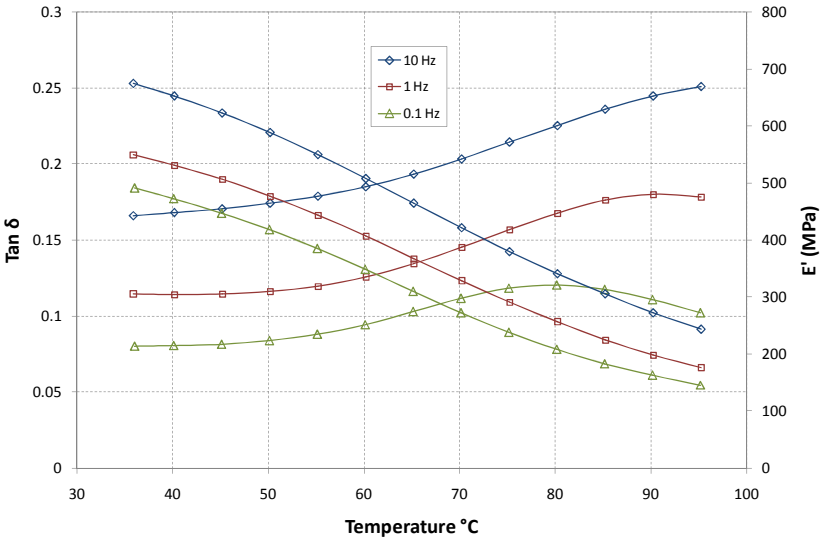

Sample 3

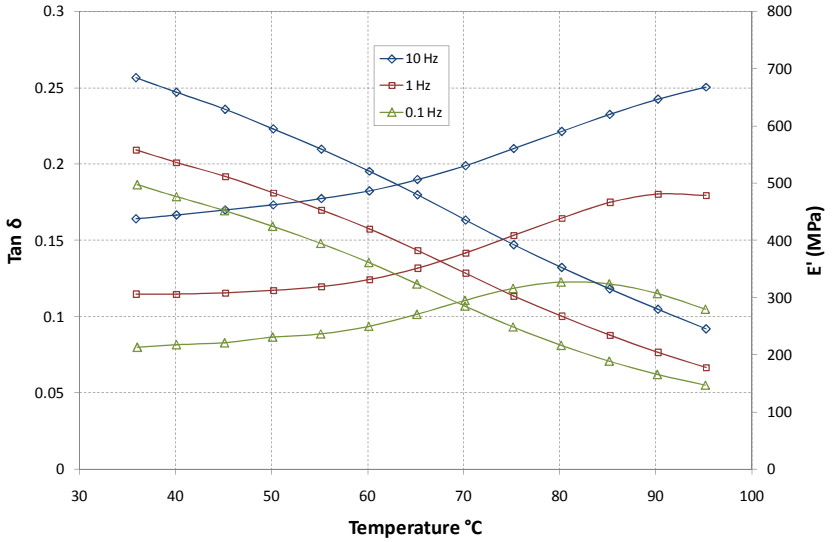

[redacted]

E.obliqua Radial Sample	Tg (°C)			
	0.1 Hz		1.0 Hz	
	Gaussian	r^2	Gaussian	r^2
1	80.2	0.999	91.8	0.999
2	79.9	0.999	91.0	0.999
3	81.2	0.997	92.3	0.999
Average	**80.4**	**0.998**	**91.7**	**0.999**

Appendix C – Shrinkage results

Corymbia citriodora (spotted gum) – sample 1 - radial / tangential

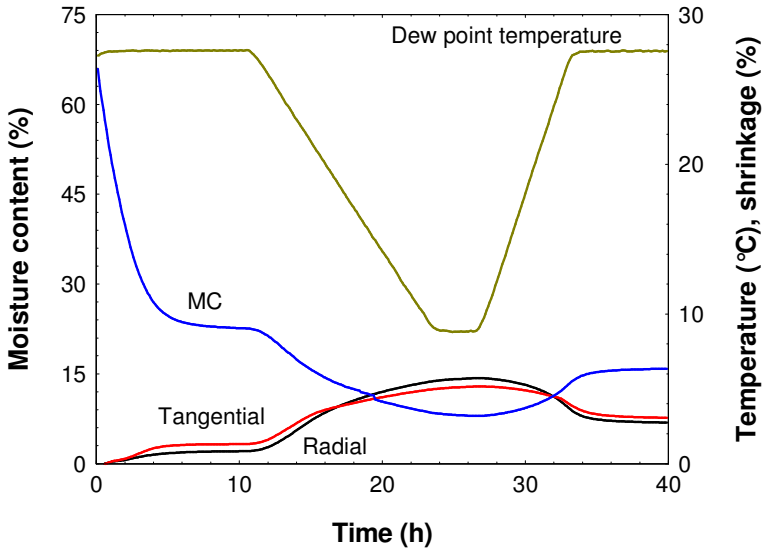

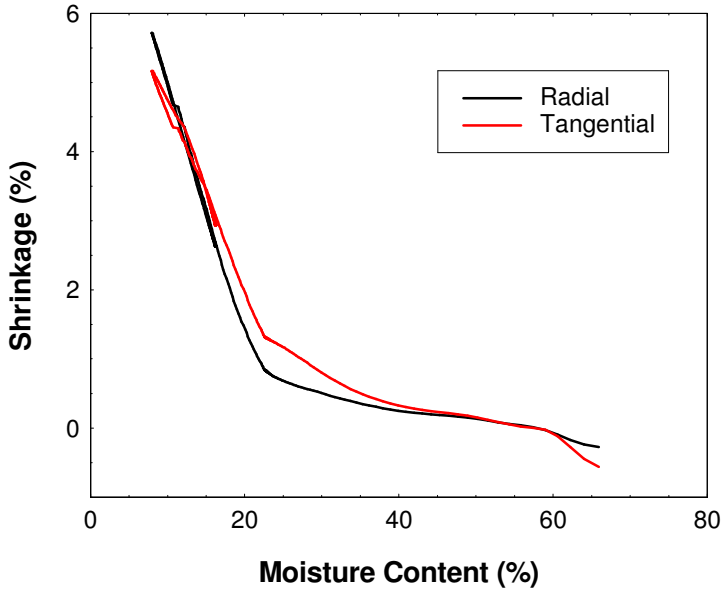

Corymbia citriodora (spotted gum) – sample 2 - radial / tangential

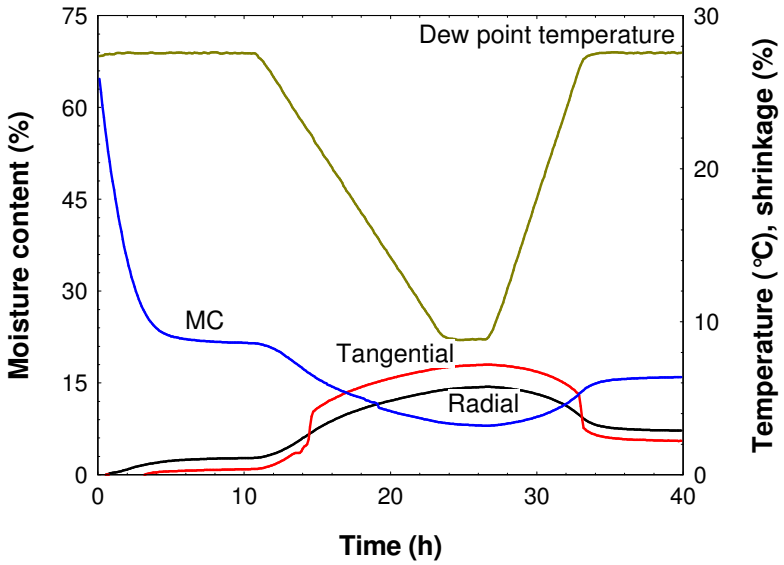

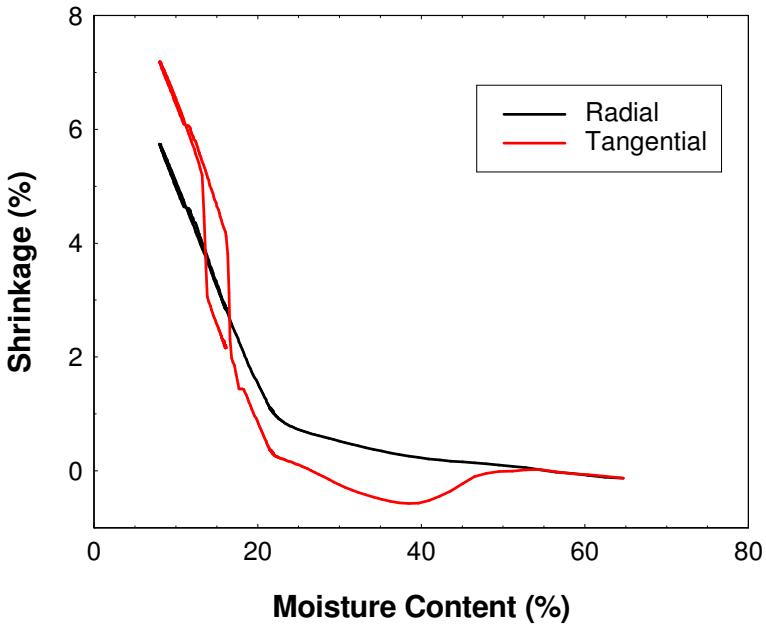

Corymbia citriodora (spotted gum) – sample 3 - radial / tangential

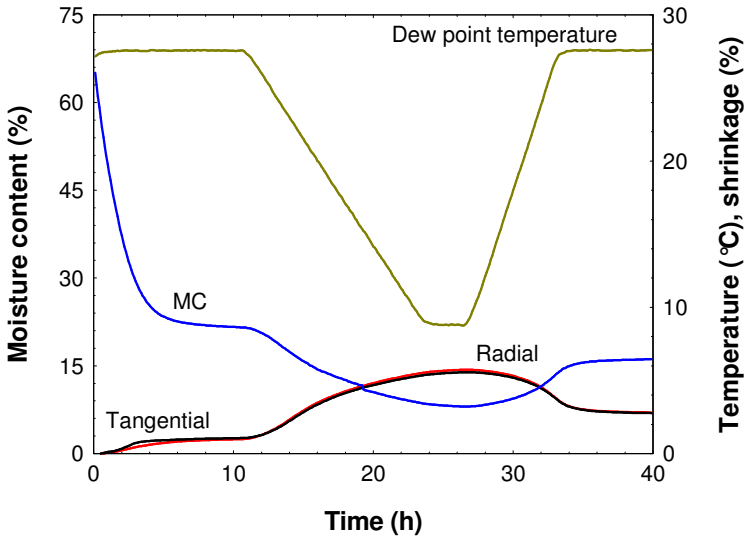

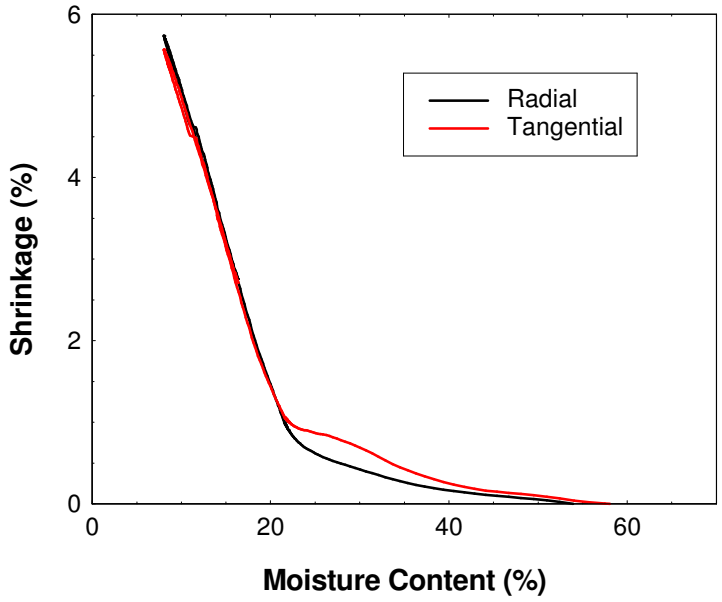

Eucalyptus marginata (jarah) – sample 1 - radial / tangential

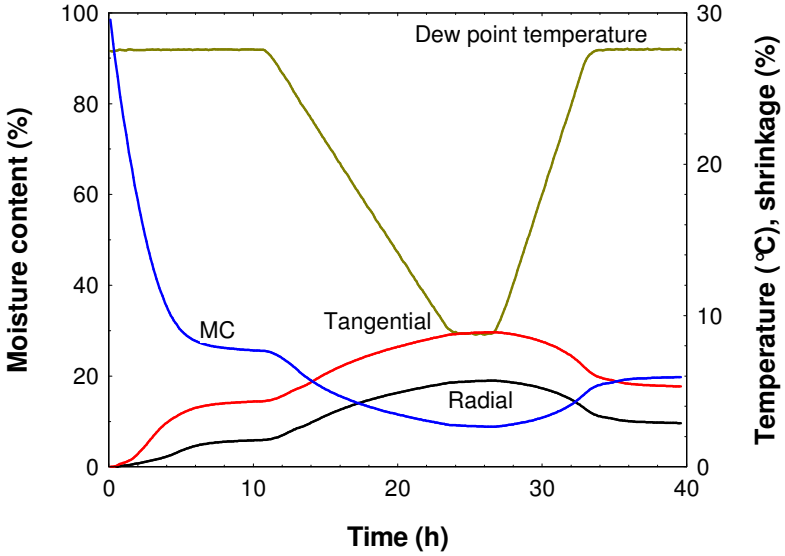

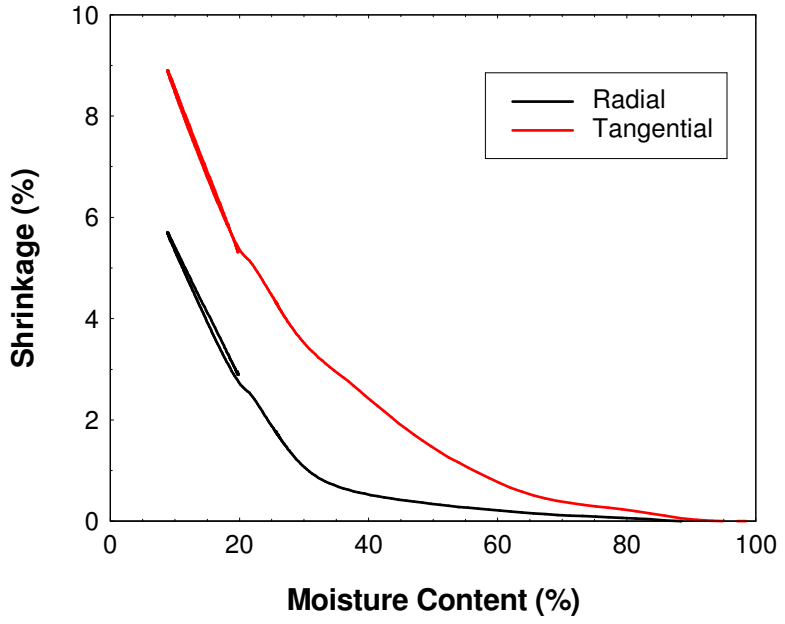

Eucalyptus marginata (jarah) – sample 2 - radial / tangential

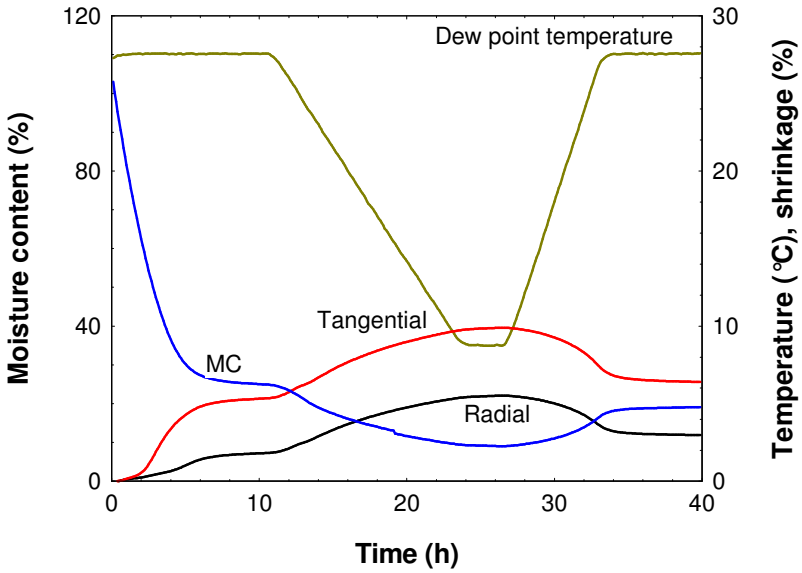

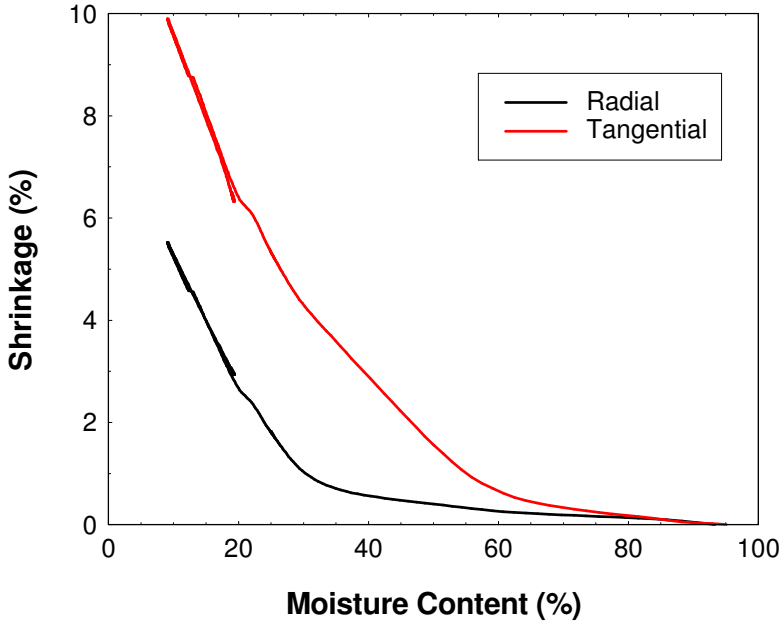

Eucalyptus pilularis (blackbutt) – sample 1 - radial / tangential

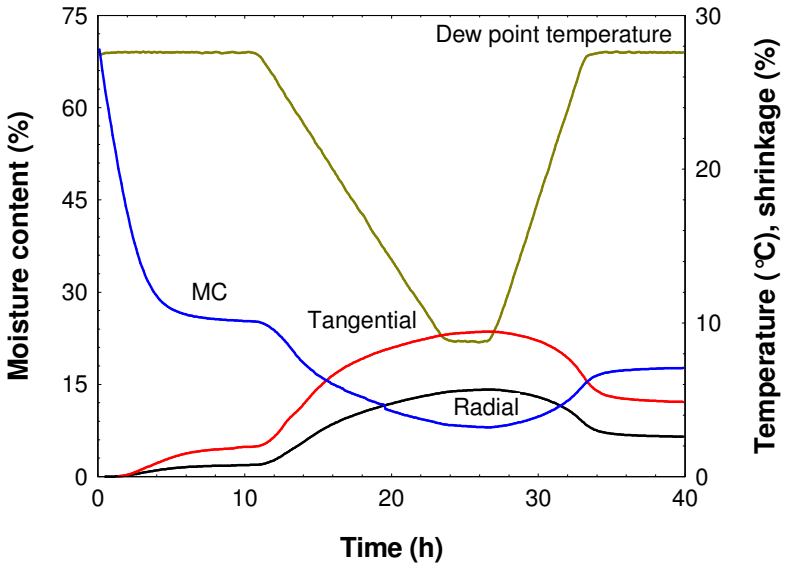

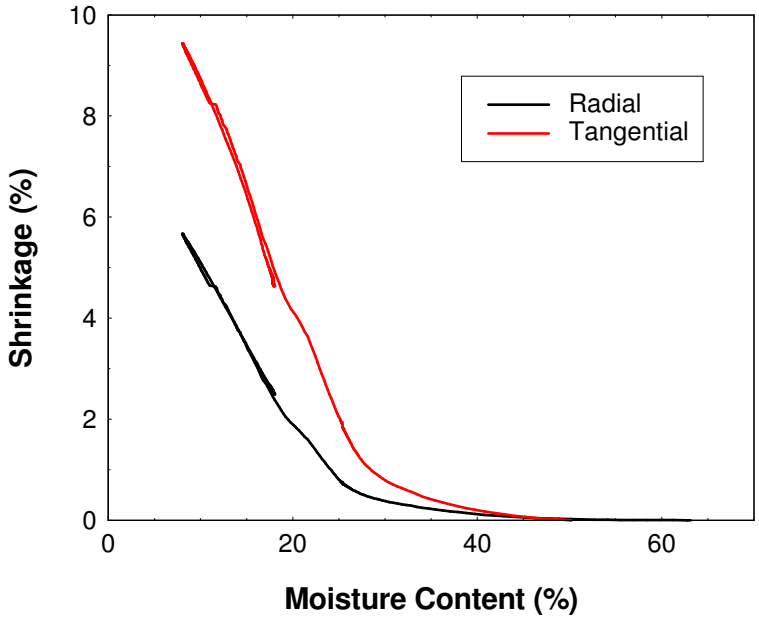

Eucalyptus pilularis (blackbutt) – sample 2 - radial / tangential

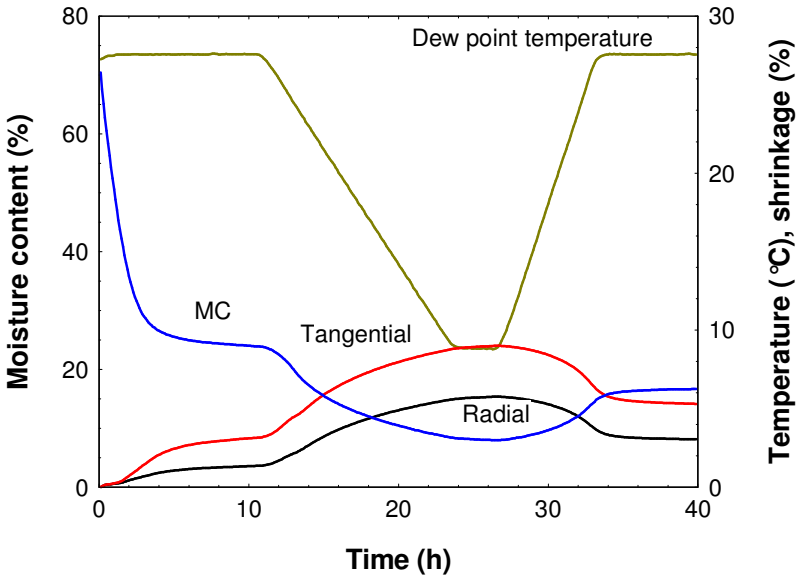

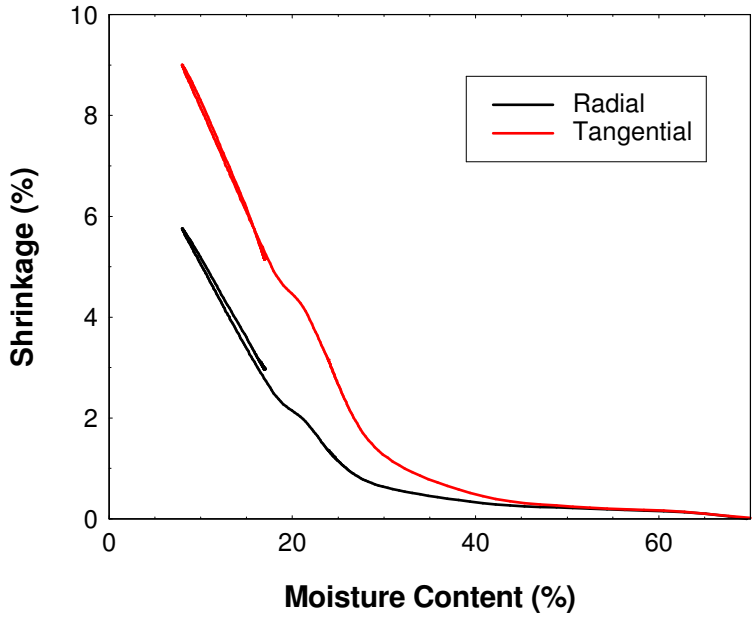

Eucalyptus obliqua (messmate) – sample 1 - radial / tangential

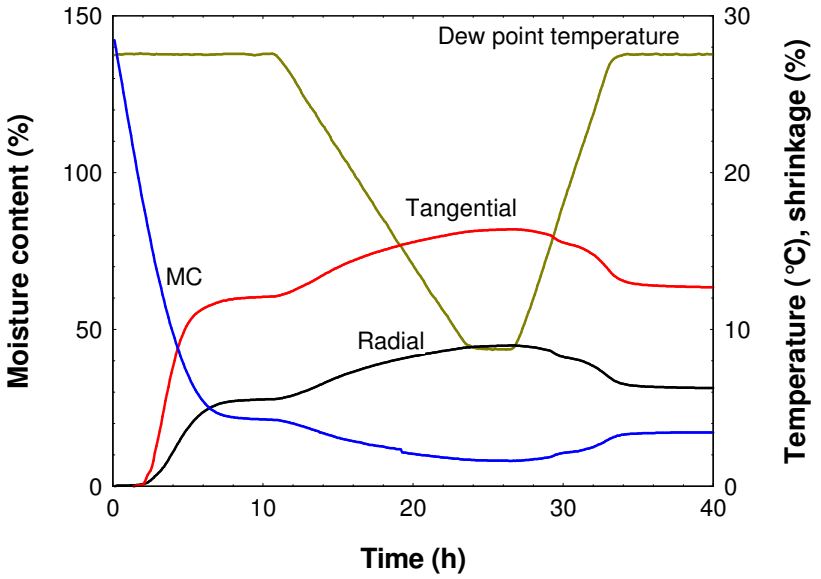

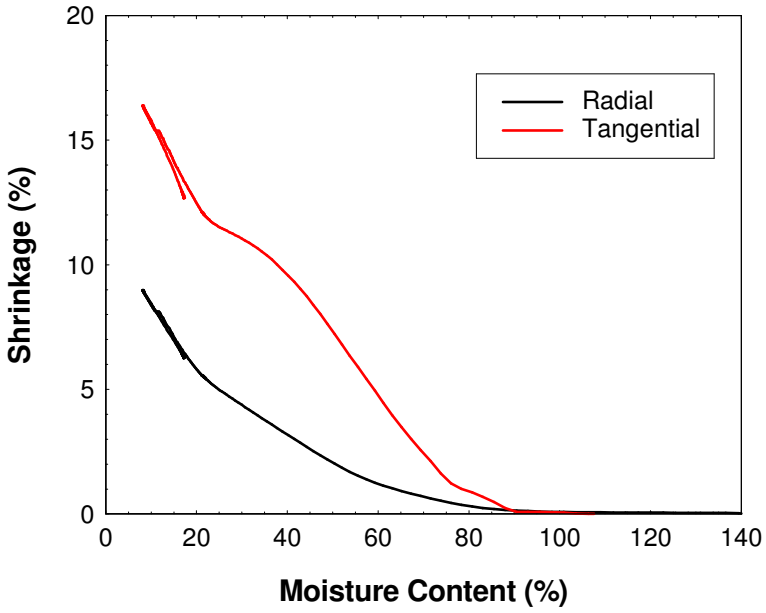

Eucalyptus obliqua (messmate) – sample 2 - radial / tangential

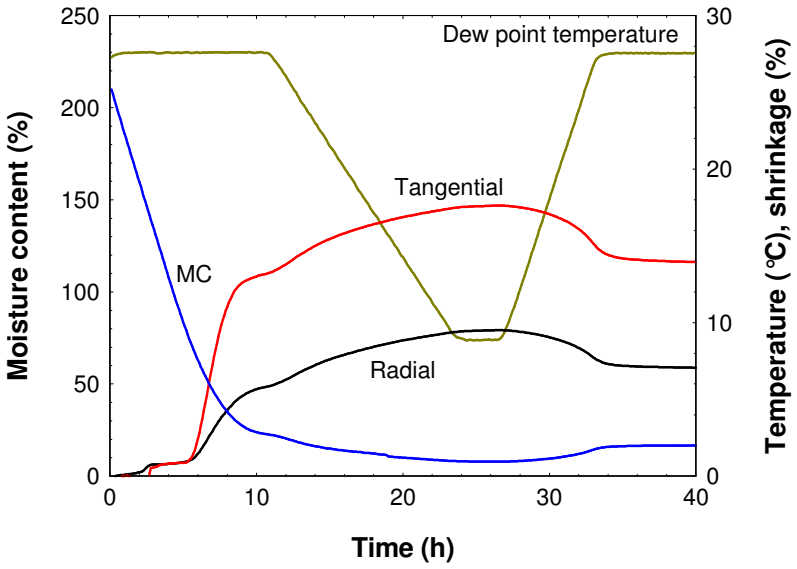

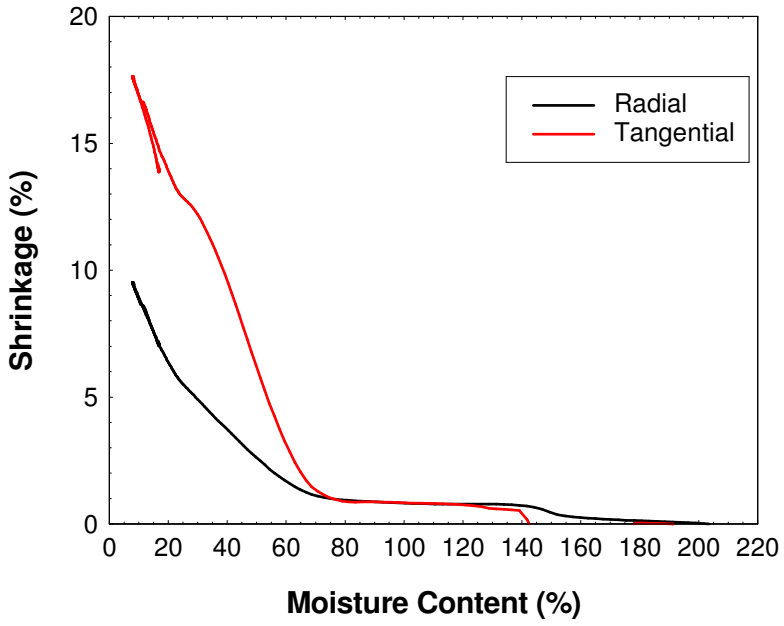

Eucalyptus obliqua (messmate) – sample 1 - longitudinal / tangential

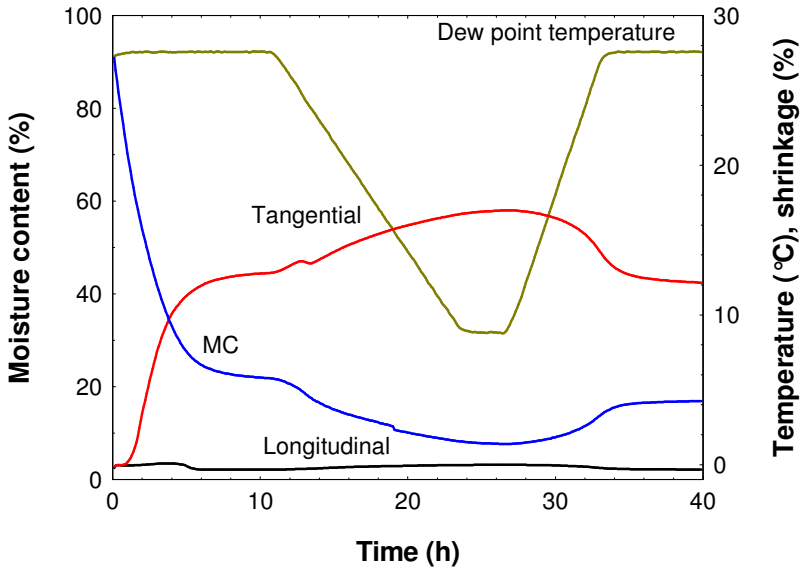

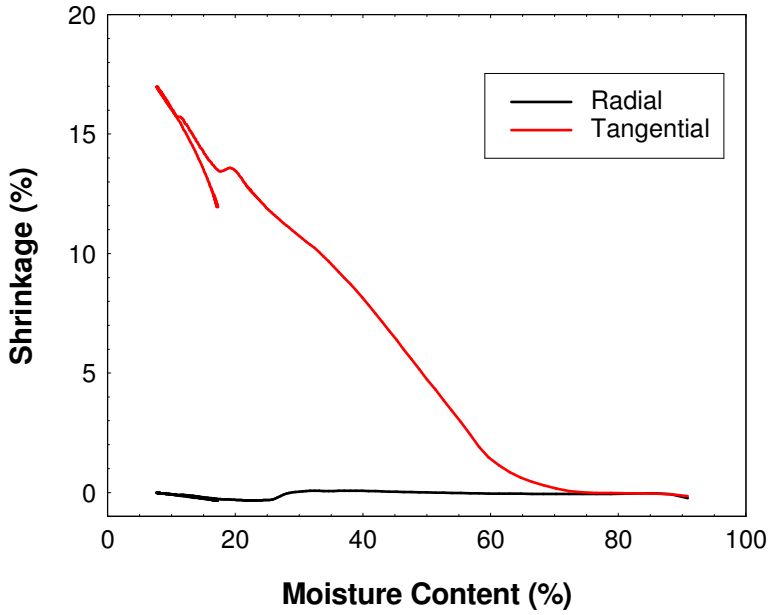

Eucalyptus obliqua (messmate) – sample 2 - longitudinal / tangential